AFWAL-TR-88-3022

AD-A196 744

MODIFICATION OF AN UNSTEADY TRANSONIC SMALL DISTURBANCE PROCEDURE TO ALLOW A PRESCRIBED STEADY-STATE INITIAL CONDITION

Don W. Kinsey

Aerodynamics and Airframe Branch
Aeromechanics Division

January 1988

Interim Report for Period January 1987 - January 1988

Approved for Public Release; Distribution is Unlimited

FLIGHT DYNAMICS LABORATORY
AIR FORCE WRIGHT AERONAUTICAL LABORATORIES
AIR FORCE SYSTEMS COMMAND
WRIGHT-PATTERSON AIR FORCE BASE, OHIO 45433-6553

UNCLASSIFIED

SECURITY CLASSIFICATION OF THIS PAGE

REPORT DOCUMENTATION PAGE

Form Approved OMB No. 0704-0188

1a. REPORT SECURITY CLASSIFICATION Unclassified	1b. RESTRICTIVE MARKINGS N/A
2a. SECURITY CLASSIFICATION AUTHORITY N/A	3. DISTRIBUTION / AVAILABILITY OF REPORT Approved for public release; distribution unlimited.
2b. DECLASSIFICATION / DOWNGRADING SCHEDULE N/A	
4. PERFORMING ORGANIZATION REPORT NUMBER(S) AFWAL-TR-88-3022	5. MONITORING ORGANIZATION REPORT NUMBER(S) N/A
6a. NAME OF PERFORMING ORGANIZATION AFWAL 6b. OFFICE SYMBOL (If applicable) FIMM	7a. NAME OF MONITORING ORGANIZATION N/A
6c. ADDRESS (City, State, and ZIP Code) Wright-Patterson AFB OH 45433-6553	7b. ADDRESS (City, State, and ZIP Code) N/A
8a. NAME OF FUNDING / SPONSORING ORGANIZATION AFWAL 8b. OFFICE SYMBOL (If applicable) FIMM	9. PROCUREMENT INSTRUMENT IDENTIFICATION NUMBER N/A
8c. ADDRESS (City, State, and ZIP Code) Wright-Patterson AFB OH 45433-6553	10. SOURCE OF FUNDING NUMBERS PROGRAM ELEMENT NO. 62201F; PROJECT NO. 2404; TASK NO 10; WORK UNIT ACCESSION NO. A1

11. TITLE (Include Security Classification)
(U) Modification of an Unsteady Transonic Small Disturbance Procedure to Allow A Prescribed Steady-State Initial Condition

12. PERSONAL AUTHOR(S)
Don W. Kinsey

13a. TYPE OF REPORT	13b. TIME COVERED	14. DATE OF REPORT (Year, Month, Day)	15. PAGE COUNT
Interim	FROM Jan 87 TO Jan 88	Jan 88	61

16. SUPPLEMENTARY NOTATION
N/A

17. COSATI CODES		
FIELD	GROUP	SUB-GROUP
01	01	
01	02	

18. SUBJECT TERMS (Continue on reverse if necessary and identify by block number)
Unsteady Aerodynamics, Small Disturbence Methods, Transonic Aerodynamics, Potential Flow

19. ABSTRACT (Continue on reverse if necessary and identify by block number)

Many attempts have been made to extend the useful range of the two-dimensional, unsteady transonic small disturbance procedure, called LTRAN2. This report describes another such extension. LTRAN2 modifications are described that allow the procedure to determine the geometry corresponding to a prescribed pressure distribution. This new geometry would account for all compressible and viscous effects, and would, therefore, be a much better starting point for the unsteady calculations.

We have presented the transonic small disturbance governing equations and boundary conditions. Then the modifications required for the inverse geometry definition are described. Results for three different airfoils (NACA 0012, NACA 64A010, and NLR 7301) are presented and discussed. The NACA 0012 and NLR 7301 results are much improved using the procedure described in this report. Finally, a brief summary of these and other results and recommendations for additional work is provided.

20. DISTRIBUTION / AVAILABILITY OF ABSTRACT	21. ABSTRACT SECURITY CLASSIFICATION
☒ UNCLASSIFIED/UNLIMITED ☐ SAME AS RPT ☐ DTIC USERS	Unclassified

22a. NAME OF RESPONSIBLE INDIVIDUAL	22b TELEPHONE (Include Area Code)	22c OFFICE SYMBOL
DON W. KINSEY	513-255-2481	AFWAL/FIMM

DD Form 1473, JUN 86 *Previous editions are obsolete.*

SECURITY CLASSIFICATION OF THIS PAGE

UNCLASSIFIED

FOREWORD

This report was prepared by Don W. Kinsey of the Aerodynamics and Airframe Branch, Aeromechanics Division, Flight Dynamics Laboratory, Wright-Patterson AFB, Ohio. The work was performed under Work Unit 240410A1.

The work was part of an effort to develop improved computational capability for predicting unsteady, transonic flows. Modifications made to an existing computer program (LTRAN2) are described and some sample results are provided.

TABLE OF CONTENTS

LIST OF ILLUSTRATIONS

LIST OF ILLUSTRATIONS

LIST OF TABLES

I. INTRODUCTION

The need for a method to determine the unsteady, transonic flow conditions over an airfoil is well established. The possible applications for such a solution method include buffet and flutter studies for fixed wing aircraft, propeller and rotor blade studies, turbine blade and guide vane designs and many more. The equations governing unsteady, transonic flow of a viscous fluid (Navier-Stokes equations) have been known for over 140 years. However, solving the equations for any practical, time-accurate transonic, viscous flow over arbitrary airfoils requires vast computer resources. Reducing the problem to two dimensions still leaves a challenging task.

Some success in solving attached flow problems has been achieved by making simplifying assumptions. Flow conditions that have very thin boundary layers can be closely approximated by inviscid equations, the so-called Euler solutions. Another major simplifying assumption is the irrotational flow assumption. This allows the definition of a velocity potential, and the combination of the equations of motion into a single equation referred to as the full potential equation. Finally, the full potential equation can be examined and, using order-of-magnitude arguments, reduced to the small disturbance equation.

Solution of the two-dimensional, transonic small disturbance (TSD) equation provides a relatively quick and inexpensive method of predicting unsteady transonic flow over thin airfoils. However, flow conditions which produce significant boundary layer growth and/or significant shock-boundary layer interactions are not well predicted by the inviscid, irrotational TSD equations. As a result, calculations which use the steady small disturbance solution as a starting point for unsteady calculations have serious inherent errors.

Information about the steady-state aerodynamics on the surface of an airfoil is often known from experimental data or may be determined with more sophisticated prediction techniques. If a new geometry

could be determined so that the TSD solution conforms to the prescribed surface aerodynamics, a much more satisfactory steady-state starting solution would be established. The effects of boundary layers, local shock-induced separation, and other flow conditions would be effectively added to the inviscid solution. Once the correct steady-state conditions are produced by the small disturbance procedure applied to the new geometry, subsequent time dependent variations should also be more representative of the real flow situation.

A numerical procedure for determining unsteady aerodynamics of two-dimensional, thin airfoils using the TSD equations was developed by NASA/Ames and given the name LTRAN2.[1-7] Several versions of LTRAN2 exist. The version used for this study has a low-frequency and a high-frequency option, a wind tunnel wall option, a boundary layer option and a lag entrainment option. An implicit algorithm is used to solve the governing equations for the flow about thin, two-dimensional bodies in oscillatory motion, plunge motion, or an oscillating flap motion.

The normal unsteady solution procedure is to first compute the steady-state potential flow about the body at a given initial angle of attack. Then, variations in the potential flow about the initial conditions are determined as a function of time for the type of motion defined.

The objective of this study is to develop a procedure that allows the user to obtain the initial surface potentials. Once the potentials are defined on the surface of the airfoil, a modified steady-state solution routine is employed in an inverse mode to obtain the geometry that would produce the target surface potentials. This new geometry is then used to compute unsteady solutions that provide much better approximations to the experimental unsteady characteristics. Experimentally measured surface static pressures or steady-state solutions from higher order flow solvers are both excellent sources of surface information for steady-state flow conditions.

This report will provide a description of the governing transonic small disturbance equations and the boundary conditions. A discussion

of the modifications necessary for the inverse steady-state procedure will be included and some representative results will be shown.

II. GOVERNING EQUATIONS AND SOLUTION SCHEME

Development of the Small Disturbance Equations

The unsteady, small disturbance flow equation is derived from the unsteady Euler equations. Assuming irrotational flow (fluid particles do not rotate about their axis) allows the Euler equations to be combined into a single equation in terms of a velocity potential, Φ. For isentropic flow, relationships exist between pressure (p), density (ρ) and speed of sound (a) so that p and ρ do not appear explicitly in the equation. This provides the full potential flow equation:

$$\frac{\partial^2 \Phi}{\partial t^2} + \frac{\partial}{\partial t}(\nabla\Phi.\nabla\Phi) + \nabla\Phi.\nabla(\frac{\nabla\Phi.\nabla\Phi}{2}) = a^2 \nabla^2\Phi$$

where,

$$a^2 = a_\infty^2 - (\gamma - 1)[\frac{\partial\Phi}{\partial t} + (1/2)(\nabla\Phi.\nabla\Phi - U_\infty^2)].$$

a_∞ = free stream speed of sound.

Further simplification of the potential equation is possible by restricting the analysis to cases were the following small disturbance assumptions are valid;

$$k,\ 1-M_\infty^2,\ \text{and}\ \tau^{2/3} << 1.$$

Where, k is the reduced frequency, = $\omega\ c/U_\infty$

c is the chord length of the airfoil,

U_∞ is the undisturbed freestream velocity,

ω is the unsteady oscillatory frequency of the airfoil,

τ is the airfoil thickness-to-chord ratio,

M_∞ is the freestream Mach number.

The resulting equation can be written in terms of a small perturbation velocity potential (ϕ) as:

$$A\,\phi_{tt} + 2\,B\,\phi_{xt} = C\,\phi_{xx} + \phi_{yy}. \qquad (1)$$

Where, $A = k^2\,M_\infty^2\,/\tau^{2/3}$

$B = k\,M_\infty^2\,/\tau^{2/3}$

$C = [(1-M_\infty^2)/\tau^{2/3}] - (\gamma+1)M_\infty^{\Omega}\,\phi_x.$

x and y are the Cartesian coordinates in the freestream and vertical directions respectively. γ is the ratio of specific heats. m is normally 2.0 (Spreiter scaling) but may vary for some applications. The subscripts on ϕ represent partial derivatives of ϕ with respect to the subscripted variable. x is nondimensionalized by c, y by $c\,\tau^{2/3}$, time by ω^{-1}, and ϕ by $c\,U_\infty\tau^{2/3}$.

LTRAN2 Description

A true high frequency solution would require the solution of equation (1). However, LTRAN2 achieves good results for a large number of cases by dropping the ϕ_{tt} term of $O[k^2]$ and solving the equation[3]

$$2\,B\,\phi_{xt} = C\,\phi_{xx} + \phi_{yy}. \qquad (2)$$

Both the low frequency and the high frequency options in LTRAN2 use equation (2). The difference between the low-frequency and high-frequency calculations of LTRAN2 is in the boundary conditions and the

expression used to compute pressure coefficients. The high frequency option includes time dependent terms of $O[k] < 1$ in the calculation of the pressure coefficients and the boundary conditions at the wake and downstream boundary.[3,4] A summary of the boundary conditions and pressure coefficient definitions is:

Variable	Low frequency	High frequency
Pressure coefficient	$C_p = -2\,\phi_x\,\tau^{2/3}$	$C_p = -2(\phi_x+k\phi_t)\tau^{2/3}$
Wake conditions	$[\phi_x] = 0$	$[\phi_x+k\phi_t] = 0$
Downstream B.C.	$\phi_x = 0$	$\phi_x+k\phi_t = 0$
Upstream B.C.	$\phi = 0$	$\phi = 0$
Upper and lower B.C.	$\phi_y = 0$	$\phi_y = 0$

where the brackets [] are used to signify this is a jump condition across the wake.

The surface tangency boundary condition for low frequencies is satisfied by

$$\phi_y = f_x(x,t) \qquad \text{for } y = 0, \quad 0 < x > 1$$

where $y = \tau^{2/3} f(x,t)$ defines the airfoil surface. However, both the low- and high-frequency options of the version of LTRAN2 used for this study solved the time dependent expression

$$\phi_y = f_x + k\, f_t(x,t). \tag{3}$$

The unsteady part of LTRAN2 was not altered for the results in this report. Rather, the algorithm for determining the steady solution was modified to operate in both an inverse or a direct mode. The modifications necessary for the inverse procedure are discussed in the next section. But first, we will discuss the steady equations and the steady solution algorithm.

LTRAN2 Steady-State Solver

The equations of interests for the steady-state case are:

$$C\,\phi_{xx} + \phi_{yy} = 0 \tag{4}$$

$$\phi_x = -0.5\, C_p\, \tau^{-2/3} \tag{5}$$

$$\phi_y = f_x(x). \tag{6}$$

Where equations (5) and (6) are defined on the airfoil surface. Equation (6) becomes unbounded at the leading edge of airfoils with a finite leading-edge radius.

The finite difference solution of the small disturbance equations are computed on a rectangular grid (Figure 1). The x-axis is in the freestream direction parallel to the airfoil chord at zero angle of attack and the y-axis is vertical, or perpendicular to the x coordinate.

An approximate factorization solution algorithm (AF2) developed by Ballhaus et al.[7] is used in LTRAN2 to compute the steady-state flow solution for equation (4). Some of the more pertinent aspects of that solution scheme are given here.

A finite difference approximation for equation (4) may be written by defining a linear operator L as:

$$L\phi = (C\,\delta_{xx} + \delta_{yy})\phi - b = 0. \tag{7}$$

The matrix operator L contains δ_{xx} and δ_{yy}, which are second central difference operators in x and y respectively. It also contains C which, for purposes of analysis is considered a constant. The vector b results from boundary conditions and the vector ϕ is the exact solution to the finite difference matrix equation (7).

A general form for a two-level iterative solution procedure for equation (7) is

$$N\,D^n + \sigma\,R^n = 0 \tag{8}$$

where $D^n = \phi^{n+1} - \phi^n$ is the correction to ϕ^n after n iterations; $R^n = L\,\phi^n = (C\,\delta_{xx} + \delta_{yy})\phi^n - b$ is the residual at iteration level n; and σ is a relaxation parameter.

The proper choice of N is the key to convergence acceleration. Two guidelines for the choice of N have been established: (1) N should be chosen to resemble L as closely as possible, and (2) the matrix operations required to obtain the correction vector should be simple. An expression of N as an approximate "factorization" of L is,

$$N = N_1 \cdot N_2 \tag{9}$$

where factors N_1 and N_2 are chosen so that their product is an approximation to L. N_1 and N_2 must also be chosen so that the solution procedure is stable. Each factor may have a bidiagonal or tridiagonal form.

An approximate factorization of equation (7) that has the necessary characteristics can be written[7] as:

$$(\beta - C\,\vec{\delta}_x)(\beta\,\overleftarrow{\delta}_x - \delta_{yy})D^n = \beta[(C\,\delta_{xx} + \delta_{yy})\phi^n - b] \tag{10}$$

where $\vec{\delta}_x$ and $\overleftarrow{\delta}_x$ are first order accurate forward and backward difference approximations, respectively; and β is a parameter to be defined later. Note that equation (10) is for subsonic flow. For supersonic flow ($C > 0$), backward differences are used for δ_{xx} and δ_x.

Equation (10) can be rewritten in the form

$$\text{Step 1: } (\beta - C\,\vec{\delta}_x)F^n = \beta[(C\,\delta_{xx} + \delta_{yy})\phi^n - b]$$

$$\text{Step 2: } (\beta\,\overleftarrow{\delta}_x - \delta_{yy})D^n = F^n \tag{11}$$

where two sweeps through the grid are required for each iteration. The first step involves a matrix solution of y = constant grid points and defines the intermediate function F^n. The second step requires a matrix solution for each x = constant line and defines the new potentials at each grid point.

Acceleration Parameters

In the approximate factorization equation (10), a free parameter β was introduced. The choice of β influences the convergence rate and, ideally, a new value of β that would provide the largest reduction in error should be selected after each iteration. Unfortunately, no procedure for defining the optimum value for β has yet been developed for transonic flow problems. Therefore, an acceleration parameter sequence is used and repeated during the iteration process. First, estimates are made of the values of β required to minimize the error growth for the high (β_h) and low (β_l) frequency extremes of the error. Then, β_h and β_l are incorporated in an array,

$$\beta_k = \beta_h[\beta_l/\beta_h]^{(k-1)/(Q-1)} \qquad k = 1,2,3....Q. \tag{12}$$

This array of acceleration parameters is used sequentially during the course of iterating the solution. An eight-element sequence is most often used (Q=8). Estimates based on a simple linear analysis provided that $\beta_h \doteq \Delta y^{-1}$ and $\beta_l \doteq 1$. The convergence rate may be improved by making small adjustments to the values of β_h and β_l, and from the use of other types of sequences.

Convergence Criteria

Some criteria are needed to assess the degree of convergence after each iteration. Typical are the residual, R^n, the correction, D^n, the aerodynamic lift coefficient, C_L, and the number of supersonic points, NSUP. Values for R^n and D^n approach zero as the solution converges, while NSUP and C_L approach a fixed value.

III. INVERSE PROCEDURE

The objective of the direct steady-state solution procedure is to compute surface pressure information from known surface slope information. The objective of the inverse method is to estimate surface slope information (and thus geometry) from known surface pressure information. A flow chart of how the steady solution procedure currently operates is shown in Figure 2.

The inverse solution procedure required several changes to the direct procedure. The major difference was in the form of the surface boundary conditions. In the direct procedure, the surface boundary conditions are Neumann type, where the normal derivative of ϕ was specified;

$$\phi_y = f_x(x)$$

where f_x is the local slope of the body. In the inverse procedure, the boundary conditions on the surface are Dirichlet type, where the value of the variable ϕ itself is specified. Both of these boundary conditions represent a well-posed problem that has a unique solution.

Defining Surface Conditions

The first step in the inverse procedure was to define the ϕ distribution on the surface. This was accomplished by converting the input pressure coefficients (known from experiment or higher order computation) into surface potentials by using the relationship of equation (5)

$$\phi_x = (\vec{\delta}_x)\phi = -0.5\ \tau^{-2/3}\ C_p$$

where,

$$(\vec{\delta}_x)\phi_j \equiv (\phi_{j+1} - \phi_j)/(x_{j+1} - x_j) = -0.5\ \tau^{-2/3}\ C_{p_j}.$$

Solving for ϕ_{j+1},

$$\phi_{j+1} = -0.5\ \tau^{-2/3} C_{p_j} (x_{j+1} - x_j) + \phi_j . \tag{13}$$

j is the grid index in the x direction.

Once an initial estimate for ϕ at x = 0 was determined, the remaining values at each grid point (j) along the body were computed from equation (13). The results presented in this report use the value of ϕ at the leading edge (x=0) obtained from an initial direct solution on the input geometry. Note that ϕ_x was approximated by a forward difference. A central difference approximation for ϕ_x was also run, but there was no obvious improvement in the results, and it had the disadvantage of requiring two initial values for ϕ at the leading edge.

With both ϕ and ϕ_x defined on the surface, it was a simple matter to define the second derivative of ϕ in the x direction on the surface.

$$\phi_{xx_j} = (\phi_{j-1} - 2\ \phi_j + \phi_{j+1}) / [0.5(x_{j+1} - x_{j-1})]^2 \tag{14}$$

Again, several different approximations for ϕ_{xx} are possible, but the central difference appeared to work best for the cases presented in this report.

The AF2 procedure used for steady solutions in LTRAN2 requires an estimate for ϕ_{yy} at each grid point on the surface for each y = constant sweep iteration. The direct method computes ϕ_{yy} from the known surface slope and the latest approximation for ϕ at the first grid point off the surface,

$$\phi_{yy_I} \tilde{=} (\phi_{y_{I+1}} - f_{x_I}) / (y_{I+1} - y_I) \tag{15}$$

where I is the surface grid line, and equation (6) is the relationship between f_x and ϕ_y. Equation (15) is essentially a forward difference approximation for the second derivative, but has the advantage of needing information from only one grid level away from the surface of the body (level I+1).

The inverse solution must employ another procedure for estimating the second derivative of ϕ in the y direction. Second- and third-order forward difference approximations were tried, but were unsatisfactory. Very large gradients can exist in the y direction, particularly near the leading edge of the airfoil, and the forward difference may not provide a good approximation. For example, the three term approximation for ϕ_{yy};

$$\phi_{yy_I} = (\phi_I - 2\,\phi_{I+1} + \phi_{I+2}) / [0.5(y_{I+2} - y_I)]^2$$

has errors of the order

$$(y_{I+1} - y_I)(\phi_{yyy_I})$$

which may not be a small value when large gradients exist. Also, the values for ϕ on the surface are fixed, while the values away from the surface are evolving during each iteration.

Following the example of Fung and Chung[8], the small disturbance equation itself (equation (4)) was used to solve for ϕ_{yy} at the surface;

$$\phi_{yy} = -C\,\phi_{xx}.$$

Substituting for C, the expression becomes;

$$\phi_{yy} = -\phi_{xx}[(1-M_\infty^2)\tau^{-2/3} - (\gamma+1)M_\infty^m\,\phi_x] \qquad (16)$$

Note that this approach may produce inconsistent results just above the surface. This could contribute to the problems with convergence discussed later in this section.

Equation (16) is easily solved at each grid point on the surface during the y = constant sweep of the two step iteration process. During the x = constant sweeps, the code was modified to skip the lines of code that redefine the values of ϕ on the surface.

Defining the New Geometry

After the inverse process has converged, the potential ϕ is known at each point in the domain defined by the grid system. However, the desired information is the shape of the body that would produce this potential distribution when input to LTRAN2 and solved in the direct mode. Equation (6) provides a relationship between the potentials and the surface slopes;

$$y' \equiv \partial y/\partial x = f_x(x) = \phi_y = (\phi_{I+1}-\phi_I)/(y_{I+1}-y_I) \qquad (17)$$

Starting with y=0 at x=0 (the leading edge of the airfoil), a Taylor series approximation provides an estimate for y at the next grid point;

$$y_j = y_{j-1} + y'_{j-1}(x_j-x_{j-1}) + y''_{j-1}(x_j-x_{j-1})^2/2 +$$

$$y'''_{j-1}\,(x_j-x_{j-1})^3/6 + \ldots\ldots \qquad (18)$$

Where, y'_{j-1} is computed from equation (17), and

$$y''_{j-1} \equiv \partial(y')/\partial x = \partial(\phi_y)/\partial x = (\phi_{y_j}-\phi_{y_{j-1}})/(x_j-x_{j-1}),$$

with similar approximations for higher derivatives.

Geometries were computed using both three and four terms of the Taylor series approximation and with forward, centered and backward approximations for the y'' and y''' terms. The best results were obtained using the first three terms of the Taylor series, and a forward difference approximation for y'.

$$y_j = y_{j-1} + \phi_{y_{j-1}}(x_j - x_{j-1}) + 0.5(x_j - x_{j-1})^2$$
$$[(\phi_{y_j} - \phi_{y_{j-1}})/(x_j - x_{j-1})]$$

or, after simplification,

$$y_j = y_{j-1} + 0.5(x_j - x_{j-1})(\phi_{y_j} + \phi_{y_{j-1}}) \qquad (19)$$

A new geometry is created by successively applying equation (19) at each grid point, starting at the leading edge and progressing to the trailing edge. Both the upper and lower surfaces are constructed independently. The new geometry should produce a pressure distribution identical to the target pressures when input to the direct method of LTRAN2. When this new geometry and the resulting steady-state starting solution were used in the unsteady mode, a much better comparison with experimental unsteady data was obtained.

Grid Spacing effects

The effect of grid spacing on the inverse solution was investigated. Reduced grid spacing in the x direction was implemented in the leading edge region, at the shock location and at the trailing edge. Both the leading edge and the shock location results with a finer grid spacing were worse than with the basic LTRAN2 grid distribution. However, additional grid points at the trailing edge did seem to help smooth the pressure data in that region. Reducing the grid spacing in the y direction at the body had a significant effect

on the results. In particular, reconstruction of the new geometry, which requires an accurate estimate of ϕ_y, was much better with the finer grid spacing. Therefore the results presented in this report used the basic LTRAN2 grid in the x direction plus two additional points at the trailing edge for a total of 113 points, 50 of which were on the airfoil. The grid extended ±200 chord lengths with Δx = 0.005 at the leading edge and Δx = 0.0028 at the trailing edge. The initial grid spacing in the y direction was 0.001 for the inverse procedure compared to the normal value of 0.01 for the direct solution. There were a total of 97 points in the y direction which extends to ±396 chord lengths. The main iteration loop used 1620 time steps for the unsteady calculations. This allowed for 4.5 complete cycles (at 360 steps per cycle) so that any transients would be out of the solution.

Convergence Characteristics

Convergence for the inverse method followed much the same pattern as for the direct method. Thin airfoils in subsonic flow converged rapidly when using the maximum correction (D^n), or change in lift coefficient (C_L) as the convergence criterion. However, the maximum residual (R^n) would decrease only about three orders of magnitude for the inverse method. Thick airfoils with strong shocks had maximum residual reductions of only three orders of magnitude for both the direct and the inverse methods. The maximum correction, number of supersonic points (NSUP), and the change in C_L all indicated good convergence after about 500 iterations.

Acceleration Parameters Used

Many different combinations of acceleration parameters were tried. The number of parameters in the sequence (Q), the low value

(β_l)and the high value (β_h) may be changed independently for each solution. The values that currently exist in the code are:

Process	Q	β_l	β_h
Direct solution on input geometry	8	1	800
Inverse solution	20	100	1000
Direct solution on target geometry	8	1	1000

There was little attempt to optimize these parameters for the limited cases run in this study. Note the relatively high value for β_l in the inverse method. The value required for convergence is much larger than the Ballhaus et al[7] estimate of 1 for the direct method, but is consistent with the findings of Chung and Fung[8].

In summary, the modifications made to LTRAN2 for this report include modifications to the AF2 routine, and the addition of four small subroutines to accommodate the inverse calculations. Subroutine CPINPT takes the target surface static pressures and interpolates to define values at the grid point locations. SURPHI computes and distributes values of ϕ at each grid point on both the upper and lower surface (equation (13)). PYYC02 determines the second derivative of ϕ in the y direction from equation (16). RECON reconstructs a target geometry based on the results of the converged inverse solution, equation (19).

IV. RESULTS AND DISCUSSION

The experimental data used for comparison in this report comes from the tests of Davis and Malcolm[9]. Two airfoils (NACA 64A010, NLR 7301) were tested over a range of transonic Mach numbers, Reynolds numbers, angles of attack and reduced frequencies. The models were oscillated harmonically about 50 percent and 40 percent chord respectively. Static pressure distributions for the upper and lower surfaces were provided for each test condition at the mean angle of attack (α_0). Dynamic pressure data were also provided at several points on the airfoil. The time-dependent data were Fourier-analyzed up to the fundamental frequency component; where the fundamental frequency component is the complex number that indicates the magnitude, and phase shift with respect to the input motion. The real part, imaginary part, magnitude and phase of the complex amplitudes, normalized by the amplitude of the input motion, were tabulated and are used for comparison with LTRAN2 results in this report. Since magnitude and phase are related to the real and imaginary parts by the complex relationship,

$$C_{P_R} + i\, C_{P_I} = C_{P_M}\, e^{i\theta},$$

only the magnitude and phase results will be shown in this report.

64A010 Airfoil

Table 1 lists the test conditions provided in this report. The first test condition represents the most severe case that a small disturbance procedure could reasonably be expected to handle. The 64A010 airfoil is 10 percent thick and has a moderately rounded leading edge. A significant region of supersonic flow is terminated by a shock. The airfoil was oscillated at a reduced frequency of 0.202. Comparison of the pressure coefficients from the experimental test

(solid line), the direct solution of LTRAN2 on the original 64A010 geometry (dashed line) and the direct solution on the new geometry that was determined by the inverse solution (Δ and +), is presented in Figure 3. These results indicate that LTRAN2 predicts the steady flow characteristics for this case with reasonable accuracy. A comparison of the original geometry in Figure 4 (solid line) and the geometry determined by the inverse procedure (+ and Δ), shows very little difference. The new geometry from the inverse solution has some sharpening of the leading edge and some thickening over the aft part of the airfoil.

The time-dependent results of LTRAN2, for both the original 64A010 geometry (BASIC LTRAN2) and the geometry that reproduces the experimental steady results (MODIFIED LTRAN2), and the experimental data from Ref. 9 are compared in Figures 5 and 6. Again, there appears to be little difference between the basic results and the new geometry results, and both compare favorably with the experimental results. Some representative pressure coefficient plots at different stages of the ocillatory motion, for the basic airfoil and the new geometry respectively, are provided in Figure 7 and 8.

NACA 0012 Airfoil

The second test case was the NACA 0012 airfoil, tested at Mach = 0.80, and 1.86 degrees angle of attack.[10] Reference 10 provides no time-dependent experimental data, but the 0012 airfoil is the archetypal test airfoil and represents a reasonable intermediate shape between the 64A010 and the NLR 7301 airfoils. This case is more severe than the previous case because the NACA 0012 is 12 percent thick, has a much larger leading edge radius and is at an angle of attack of 1.86. The pressure coefficient comparisons are presented in Figure 9. The direct solution for the NACA 0012 airfoil is obviously very different from the experimental steady data. The solution for the modified geometry agrees quite well with the experimental pressure data except for a small deviation at the shock.

Theoretically, the inverse procedure should produce a geometry that would exactly reproduce the target pressure distribution. In practice, however, it has been found that pressure data in the vicinity of a strong shock is very erratic. For example, the symbols in Figure 9 represent the pressure results after 1500 iterations of the inverse procedure. The results at only 10 iterations before (1490) and 10 iterations later (1510) show that an almost indistinguishable difference in geometry produced very different pressures (Figure 10). The predicted velocity at 60 percent chord on the upper surface varies from subsonic to supersonic with almost imperceptible changes in geometry.

The geometry provided by the inverse solution using the Figure 9 pressures is shown in Figure 11. The actual NACA 0012 geometry is much thicker and has a much more rounded leading edge than the geometry that would cause LTRAN2 to produce the target pressure distribution. The "fishtail" effect on the aft portion of the new geometry is obviously not practicable for an airfoil, but fortunately, the small disturbance routine only requires surface slopes.

The unsteady lift and pitching moment coefficients from the original and the modified geometries are compared in Figure 12. The magnitude and phase from the time-dependent calculations are shown in Figure 13. A look at the predicted pressures at various points during the oscillations, for the original and the new geometries respectively, is given in Figures 14 and 15. Several cycles were computed to allow any starting transients to dissipate. The original LTRAN2 solution is virtually invariant with angle of attack and produces none of the phase shift and complex pressure amplitudes of the modified LTRAN2 procedure.

NLR 7301 Airfoil

Pressure coefficients for the NLR 7301 airfoil are shown in Figure 16. This airfoil is 16.5 percent thick, has a very large leading edge radius and produces strong shocks followed by separation to the trailing edge on both the upper and lower surfaces. As with the

NACA 0012 example, the direct solution for the basic NLR 7301 geometry is completely wrong. The solution for the modified geometry is very good over the first 50 percent and the last 35 percent of the airfoil. However, the small disturbance procedure predicts too severe a velocity decrease across the shock. Attempts to improve the situation by changing grid spacing proved to be fruitless. It may well be an insurmountable characteristic of the small disturbance approximation. Indeed, Steger and Klineberg[11] show similar effects in their attempts to use the small disturbance equations in the design mode.

The original and inverse airfoil geometries are shown in Figure 17. Again, the large leading edge radius of the basic airfoil leads to a fishtail effect for the new geometry.

The direct solution on the original geometry results are shown in Figures 18 and 19. The original LTRAN2 results show very little change in the time-dependent pressure profiles and, therefore, very little change in the complex pressure, magnitude and phase. The Figures 18 and 19 results are for $k = 0.20$. A $k = 0.05$ case was also computed but the results were as bad as or worse than the $k = 0.20$ results.

The $k = 0.20$ results for the new geometry from the inverse procedure are presented in Figures 20 and 21. The LTRAN2 results compare favorably with the experimental results, though the magnitude of the peak values are different. The reason for the differences is not completely understood but is very likely associated with the shock strength errors.

Results for the $k = 0.05$ case are presented in Figures 22 and 23. As with the $k = 0.20$ data, the form of the results compares with the form of the experimental results, however, the agreement is not quite as good as for $k = 0.20$. Pressure coefficient plots in Figure 23 indicate that the solution in the neighborhood of the shock strongly influences the unsteady pressure results. Additional results and recommendations for further work are presented in Section V.

V. CONCLUSIONS

The steady-state solution subroutine in the unsteady small disturbance solver LTRAN2 has been modified to operate in an inverse or "design" mode. "Design" is written with quotation marks because there has been no attempt to produce a realistic airfoil shape. Rather, the objective of this inverse procedure is to provide a geometry (actually a set of upper and lower surface slopes) that causes LTRAN2 to match the known steady-state surface pressure. The unsteady results from the new geometry should be a much better approximation to the experimental unsteady results. The purpose is to expand the useful range of the small disturbance solver to both airfoils and flow conditions that violate the inviscid, irrotational, small disturbance assumptions.

Three separate airfoils were evaluated with this new procedure. First, an NACA 64A010 airfoil, tested at Mach = 0.80 and near zero angle of attack was evaluated. This condition is representative of the most severe case that a small disturbance procedure could be expected to handle. Indeed, there was little difference between the results obtained from LTRAN2 run in the normal mode and the results obtained from the modified geometry that produced steady-state pressure distributions that exactly matched experimental data. The unsteady pressure results from both approaches agreed well with experimental unsteady results.

Next, an NACA 0012 airfoil at Mach = 0.80 and α = 1.86 was investigated. The steady-state flow results indicated clearly that the LTRAN2 solution was not representative of the experimental data. Implementing the inverse procedure provided a geometry that did represent the experimental results when solved by LTRAN2. A problem of extreme sensitivity of the pressure coefficients at the shock was revealed. LTRAN2 over estimates the velocity reduction at the foot of strong shocks. There were no experimental unsteady results for comparison, but the results from the modified geometry were much more reasonable that the results from the basic NACA 0012 geometry.

The most severe test case was an NLR 7301 airfoil at Mach = 0.80 and near zero angle of attack. This 16.5 percent thick supercritical airfoil had a very large leading edge radius. The flow contained strong shocks on both surfaces. Again, the steady-state solution on the basic geometry was much different from the experimental steady-state results. The inverse procedure produced a geometry that resulted in good agreement with the experimental steady-state results except for the "overshoot" problem at the foot of the shock.

The unsteady results are compared for two different reduced frequencies; k = 0.20 and k = 0.05. The trends of the computed k = 0.20 results compared well with the trends of the experimental results. However, the magnitudes of some peak values were significantly different. The k = 0.05 results did not compare quite as well with the experimental data as the k = 0.20 results.

The k = 0.05 results from the NLR 7301 airfoil highlight two problem areas for the inverse procedure. Probably the most serious problem results from the fact that the experimental shock location moves fore and aft on the airfoil as the airfoil oscillates. However, the modified geometry has surface slopes that induce the shock for the steady-state solution, and this geometry remains fixed as the airfoil oscillates. As a result, the geometry is trying to force a rapid change in surface velocity (and thus pressure) at the wrong (except, perhaps twice during each oscillation) chord location.

The second problem area has been mentioned before and is the tendency for LTRAN2 to overshoot the velocity drop across the shock. The experimental data, at least for the NLR 7301 case investigated here, indicate a much less severe velocity drop across the shock than LTRAN2 predicts. The overshoot appears to be an unavoidable result of the LTRAN2 procedure. Some minor modifications to the code were tried but they did not improve the overshoot problem.

Before using this procedure on a routine basis, a parametric study of the acceleration parameters should be completed. It would probably be very useful to develop a procedure to vary the acceleration parameters as the solution evolves. The solutions presented in this report were obtained on a CRAY X-MP 12, with run times of about 4

minutes, and required about 156,000 words of memory. However, there was no attempt to improve the vectorization of the code or to decrease the memory requirements. Significant reductions in both run time and memory requirements should be possible. A more difficult but much more rewarding improvement would result from solving the overshoot problem at the shock. Last, but certainly not least, the development of a practical way of allowing the geometry modifications to move with the shock during the unsteady oscillations should reap tremendous benefits.

REFERENCES

1. Rizzetta, D.P., "Procedures for the Computation of Unsteady Transonic Flows Including Viscous Effects," NASA CR 166249, Jan 1982.

2. Guruswamy, P. and Goorjian, P.M., "Effects of Viscosity on Transonic-Aerodynamic and Aeroelastic Characteristics of Oscillating Airfoils," AIAA paper 83-0888-cp, Lake Tahoe, Nevada, May 1983.

3. Hessenius, K.A. and Goorjian, P.M., "A Validation of LTRAN2 with High Frequency Extensions by Comparison with Experimental Measurements of Unsteady Transonic Flows," NASA TM 81307, July 1981.

4. Houwink, R. and van der Vooren, J., "Results of an Improved Version of LTRAN2 for Computing Unsteady Airloads on Airfoils Oscillating in Transonic Flow," AIAA paper 79-1553, Williamsburg, Virginia, July 1979.

5. Ballhaus, W.F. and Goorjian, P.M., "Implicit Finite-Difference Computations of Unsteady Transonic Flows about Airfoils," AIAA Journal, vol. 15, no. 12, Dec 1977, pp 1728-1735.

6. Ballhaus, W.F. and Goorjian, P.M., "Computation of Unsteady Transonic Flows by the Indicial Method," AIAA Journal, vol. 16, no. 2, Feb 1978, pp 117-124.

7. Ballhaus, W.F., Jameson, A. and Albert, J., "Implicit Approximate Factorization Schemes for the Efficient Solution of Steady-State Transonic Flow Problems," AIAA Journal, vol. 16, no. 6, June 1978, pp 573-579.

8. Fung, K.Y. and Chung, A.W., "Computations of Unsteady Transonic Aerodynamics Using Prescribed Steady-State Pressures," J. Aircraft, vol. 20, no. 12, Dec 1983, pp 1058-1061.

9. Davis, S.S. and Malcolm, G.N., "Experimental Unsteady Aerodynamics of Conventional and Supercritical Airfoils," NASA TM 81221, Aug 1980.

10. Harris, C.D., "Two-Dimensional Aerodynamic Characteristics of the NACA 0012 Airfoil in the Langley 8-Foot Transonic Pressure Tunnel," NASA TM 81927, Apr 1981.

11. Steger, J.L. and Klineberg, J.M., "A Finite-Difference Method for Transonic Airfoil Design," AIAA paper no. 72-679, Boston, Massachusetts, Jun 1972.

Table 1

Test Conditions for LTRAN2 Solutions

Airfoil	Mach	k	X_0	R_n	α_0	α_1	C_L
NACA 64A010	0.796	0.202	0.50	1.3×10^7	-0.21	1.09	-0.029
NACA 0012	0.80	0.20	0.50	9.0×10^6	1.86	1.0	0.299
NLR 7301	0.807	0.20	0.398	1.2×10^7	0.36	0.49	0.047
NLR 7301	0.807	0.05	0.404	1.2×10^7	0.36	0.49	0.047

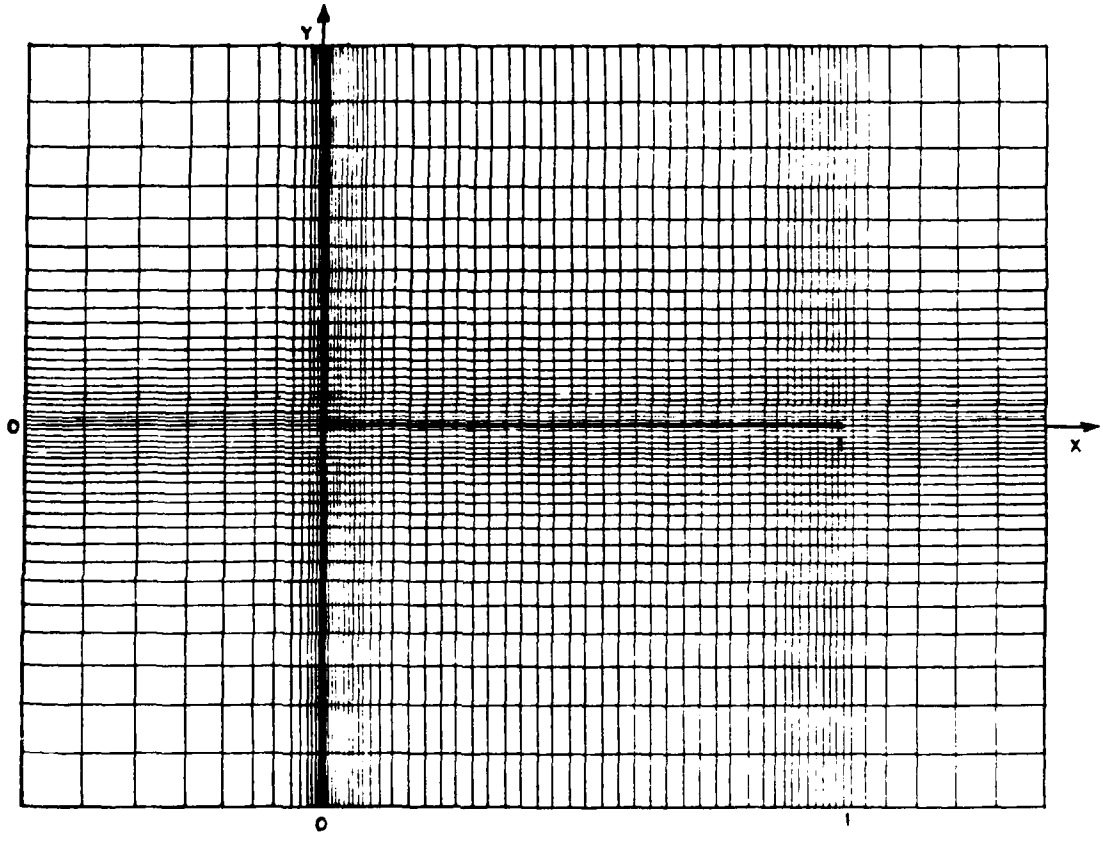

Figure 1 LTRAN2 Solution Grid Close Up

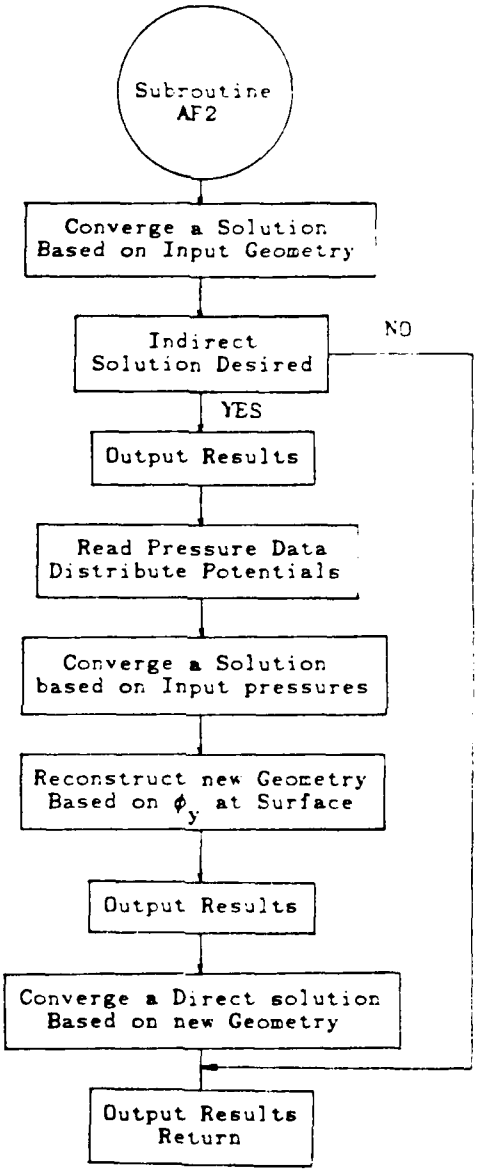

Figure 2 Modified AF2 Solution Flow Chart

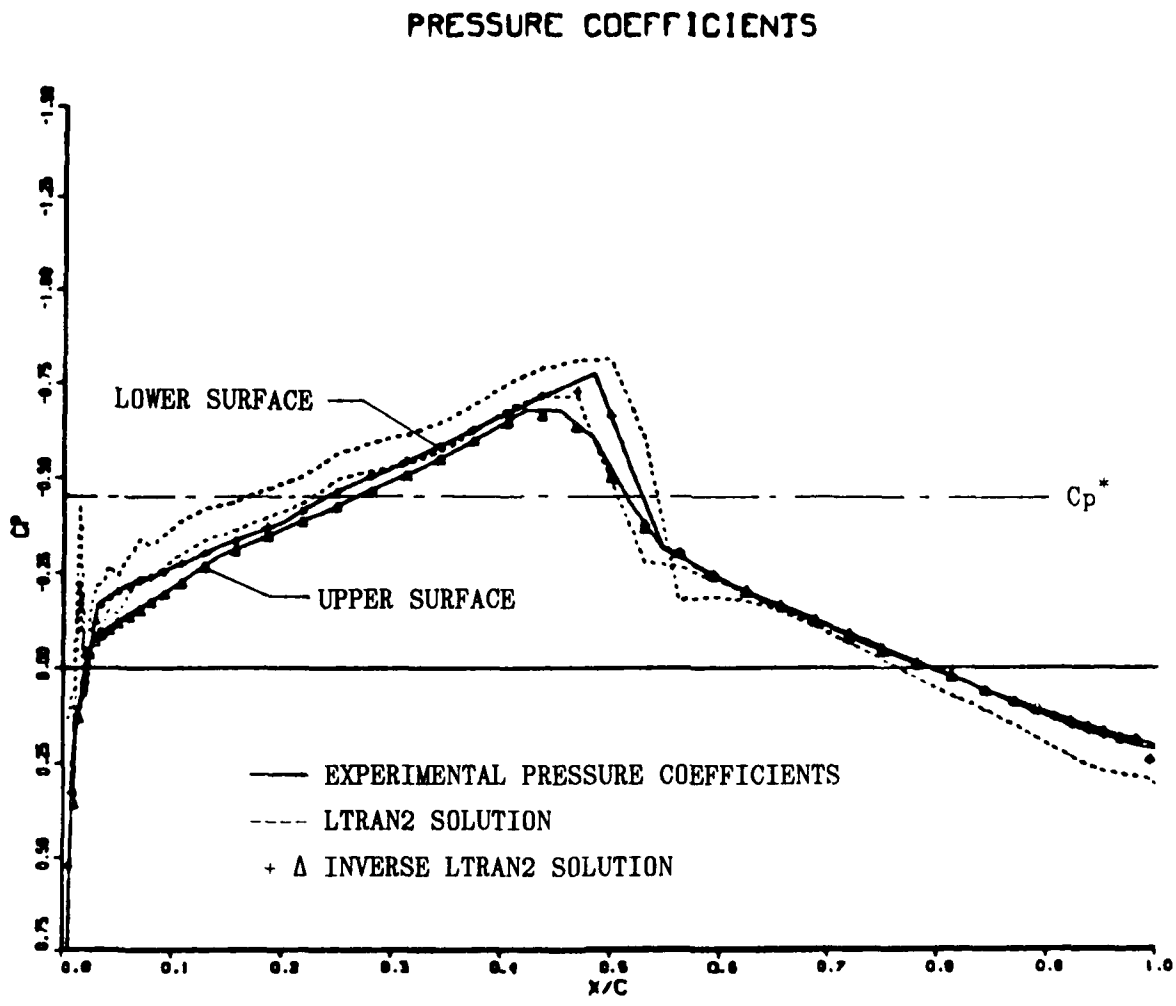

Figure 3 Pressure Coefficient Comparison, NACA 64A010, M=0.796, α = -0.21, $R_n = 1.3 \times 10^7$

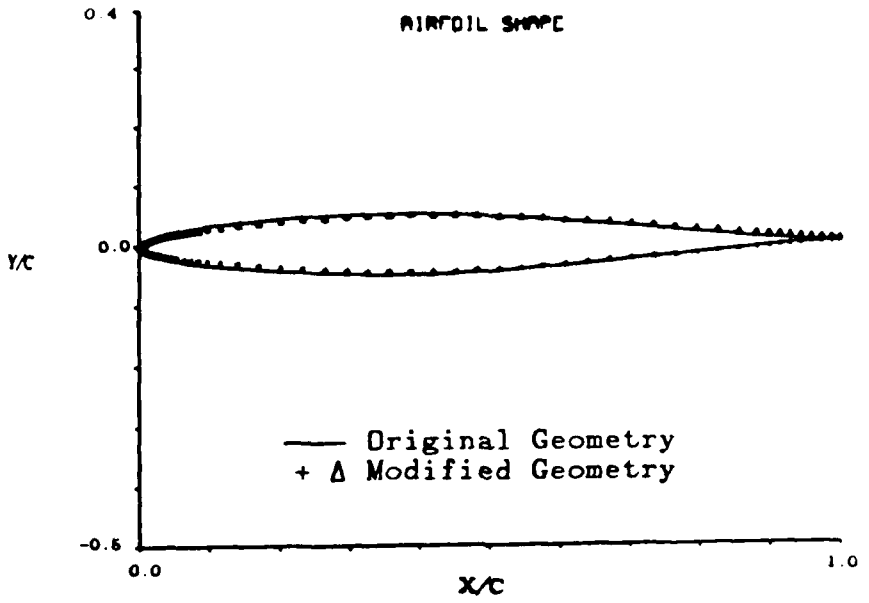

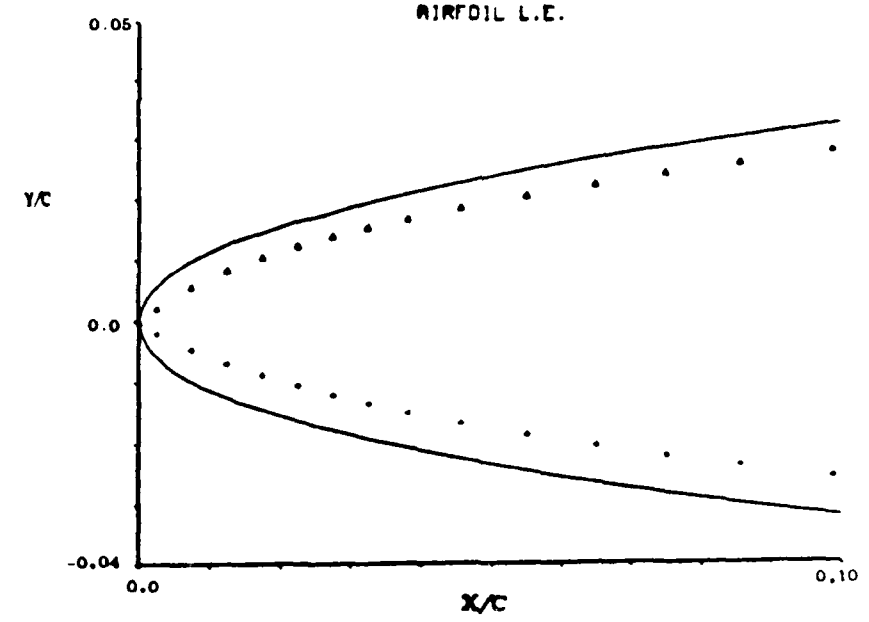

Figure 4 Geometry Comparison, NACA 64A010

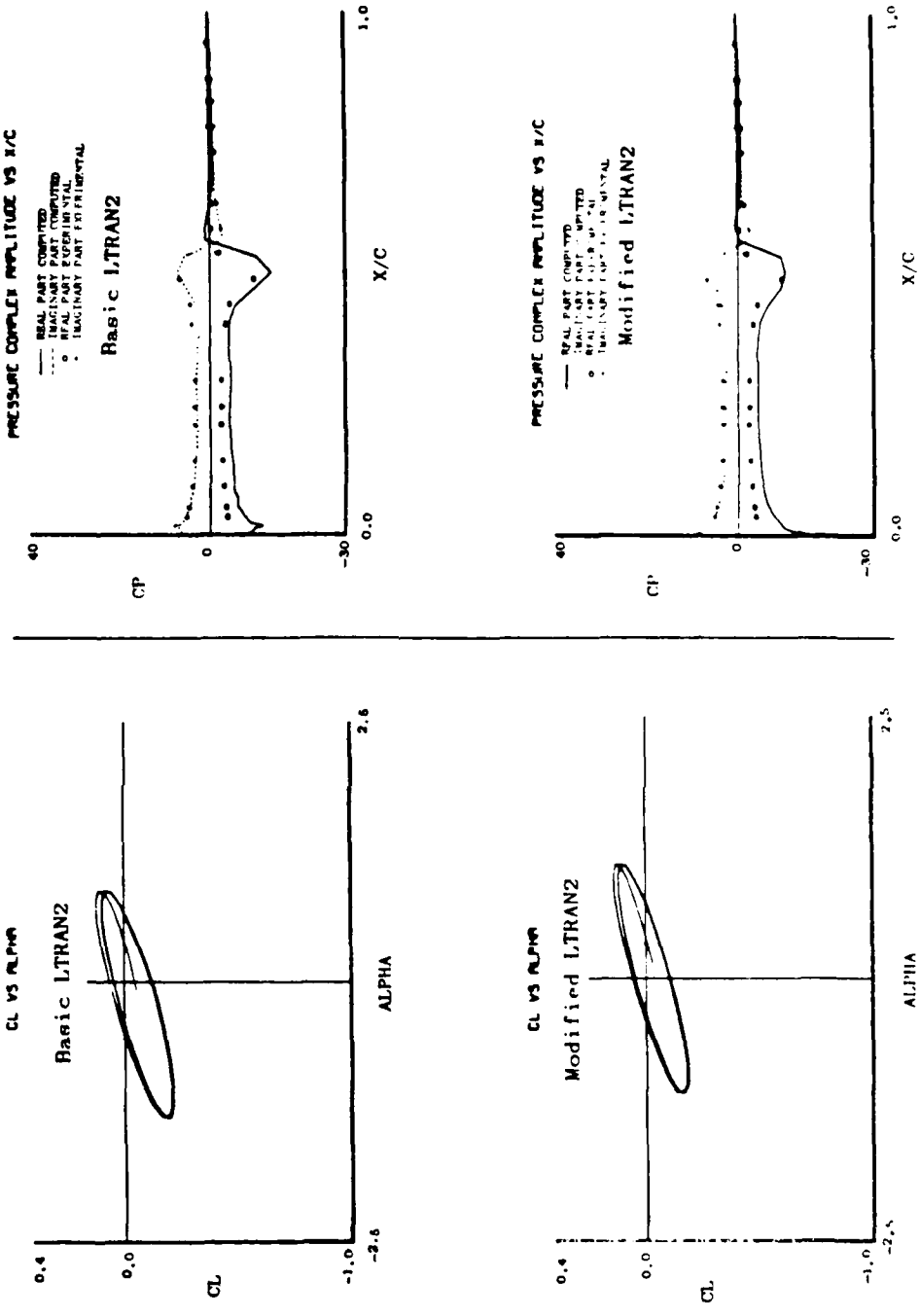

Figure 5 Comparison of Basic and Modified Geometry Results, NACA 64A010, M=0.796, k=0.202, R_n=1.3x10^7, α=-0.21+1.09 SIN ωt

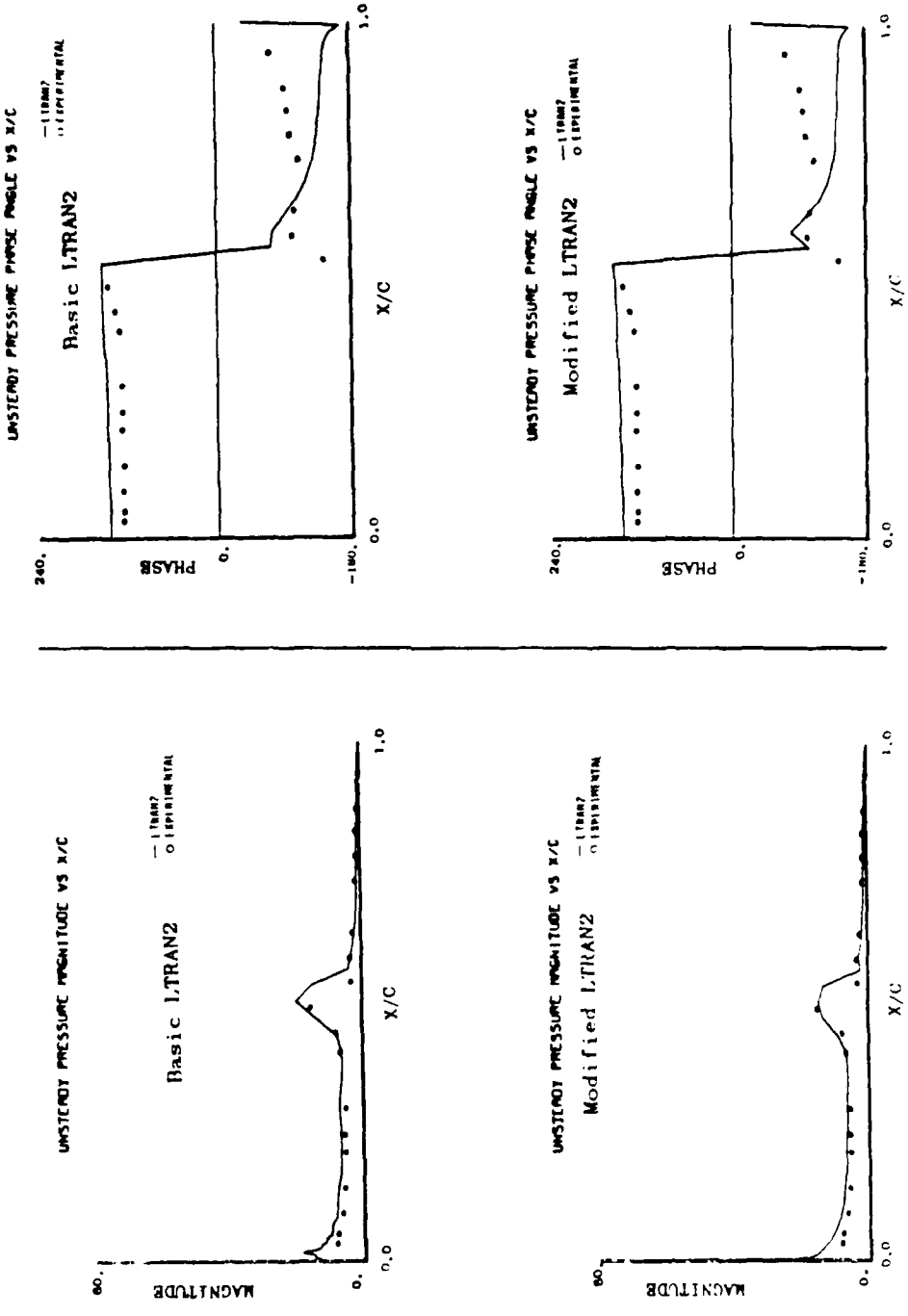

Figure 6 Comparison of Basic and Modified Geometry Results, NACA 64A010, M=0.796, k=0.202, R_n=1.3x10^7, α=-0.21+1.09 SIN ωt

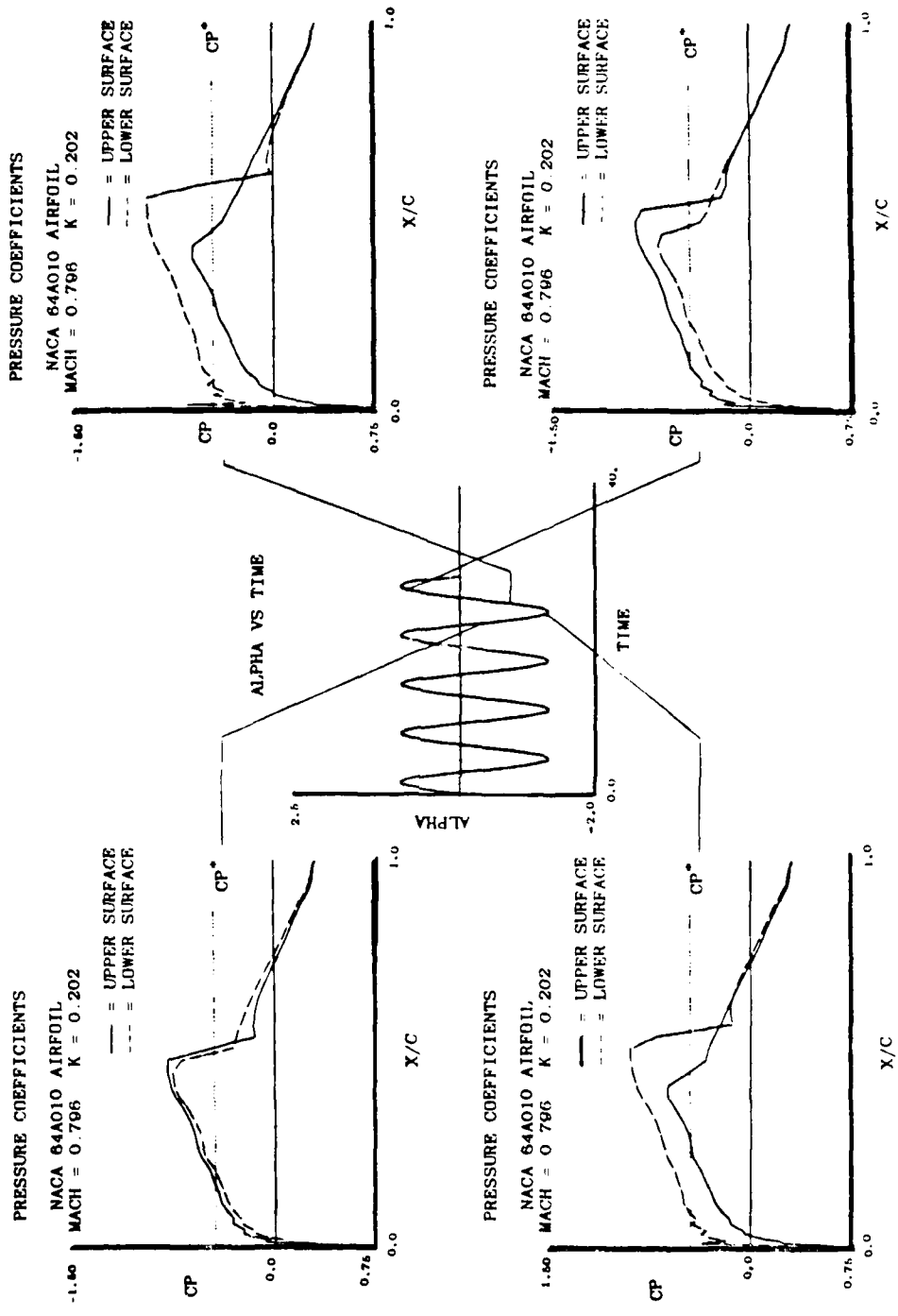

Figure 7 Basic 64A010 Geometry Time-Dependent Results

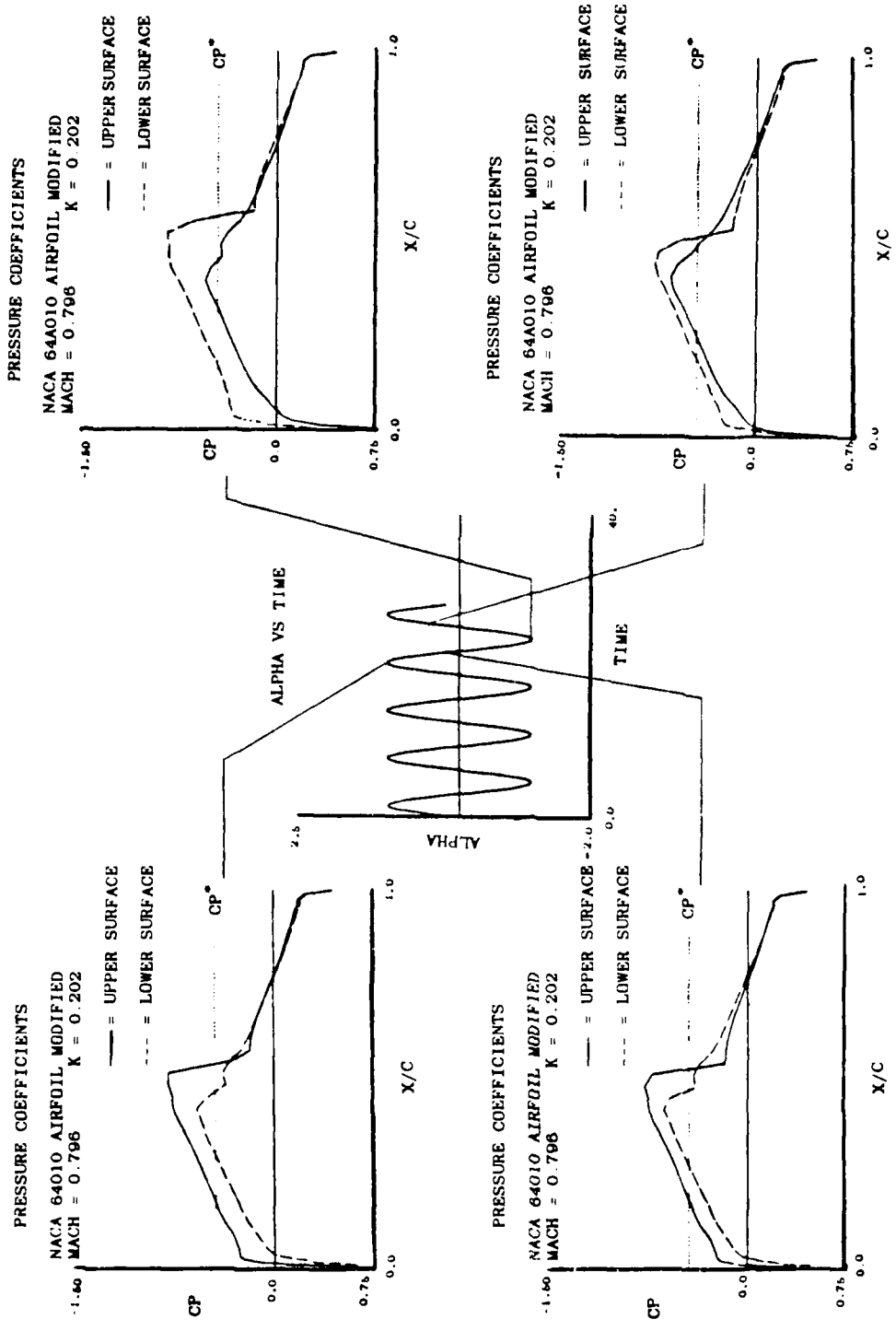

Figure 8 Modified 64A010 Geometry Time-Dependent Results

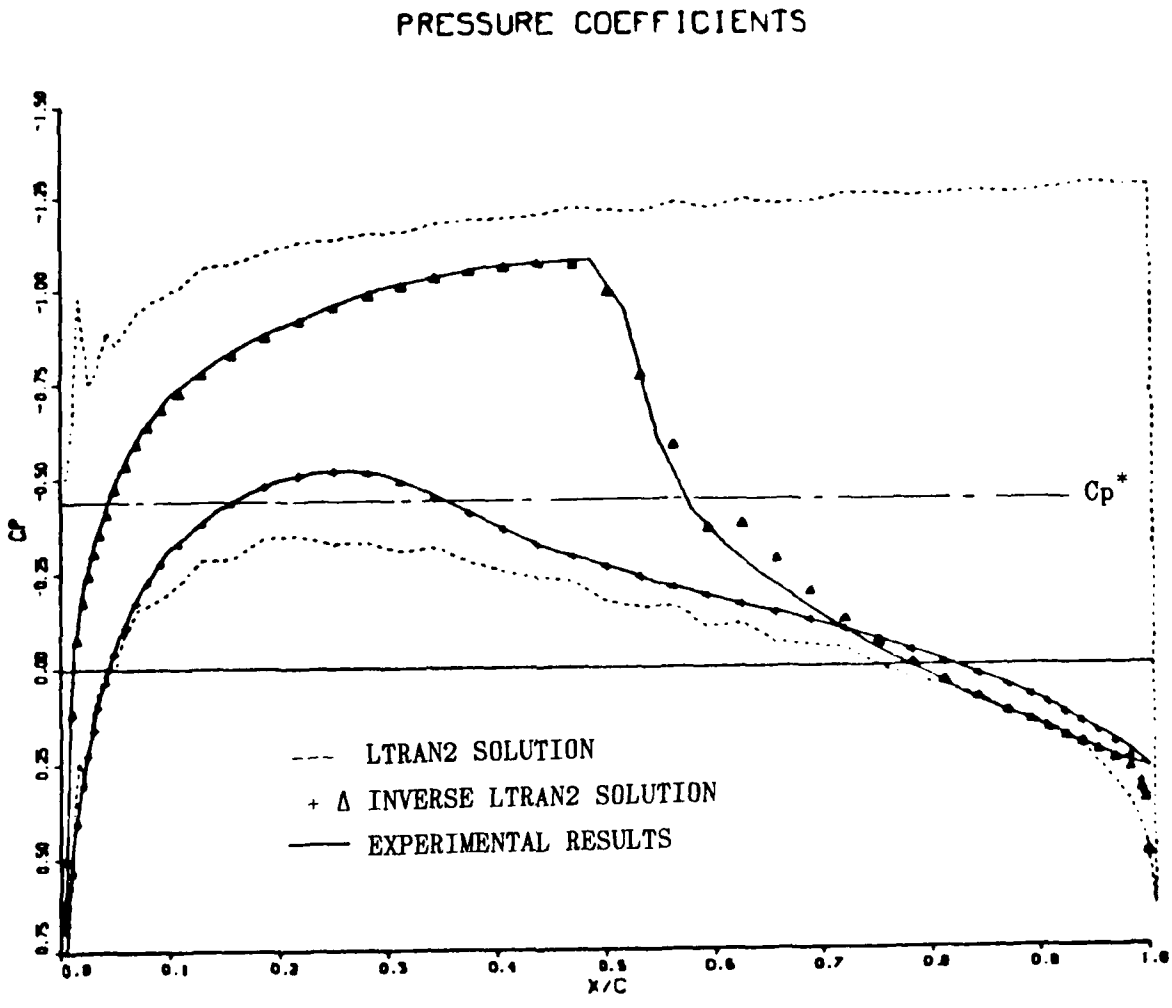

Figure 9 Pressure Coefficient Comparison, NACA 0012, M=0.80, α = 1.86, R_n= 9.0x10^6

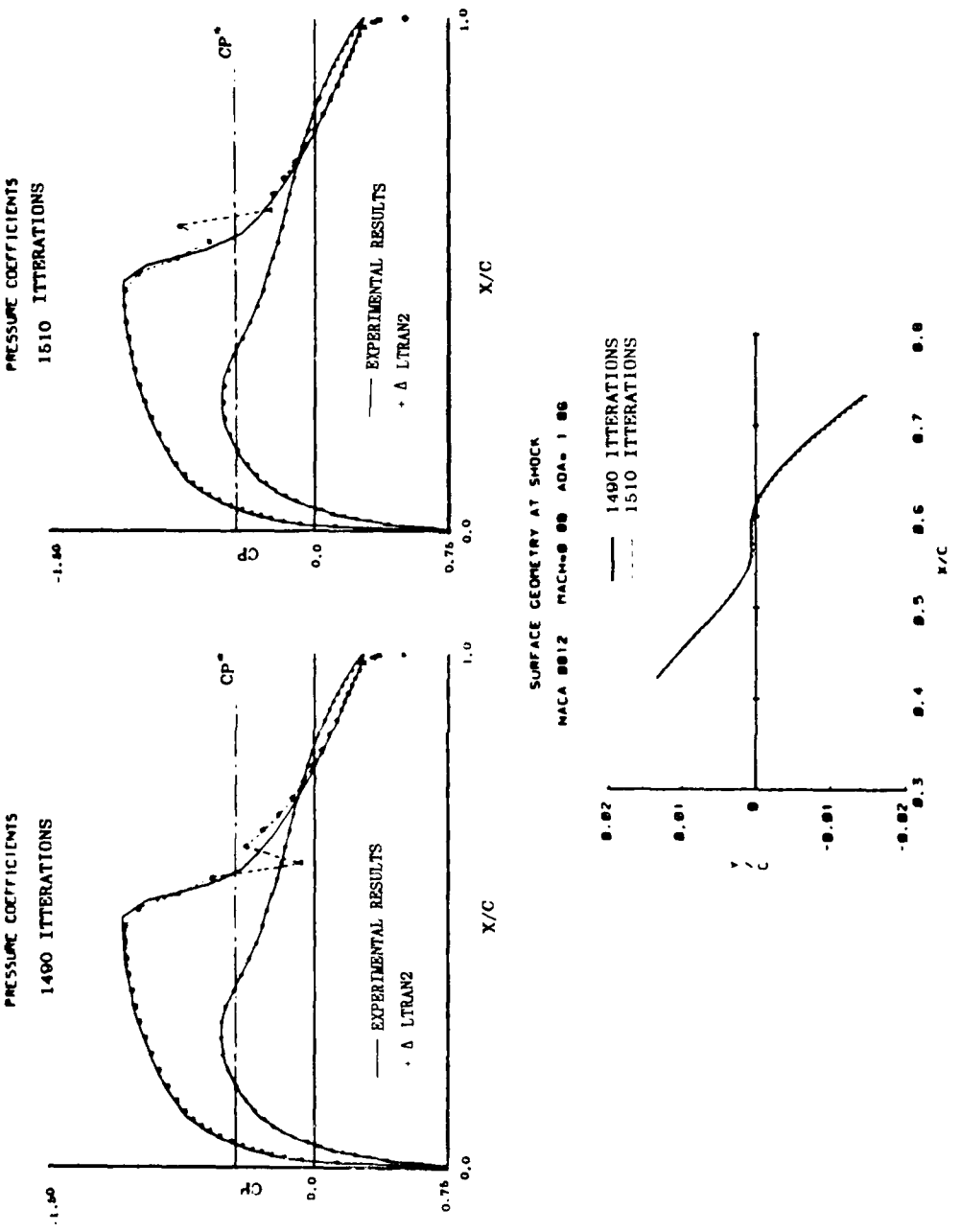

Figure 10 Sensitivity of LTRAN2 at the Shock, NACA 0012, M=0.80, α = 1.86, R_n= 9.0x10^6

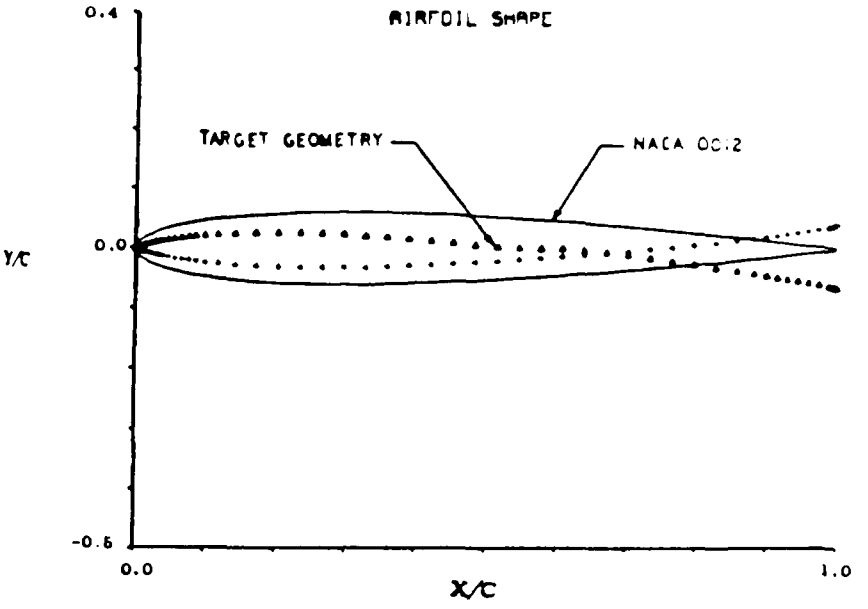

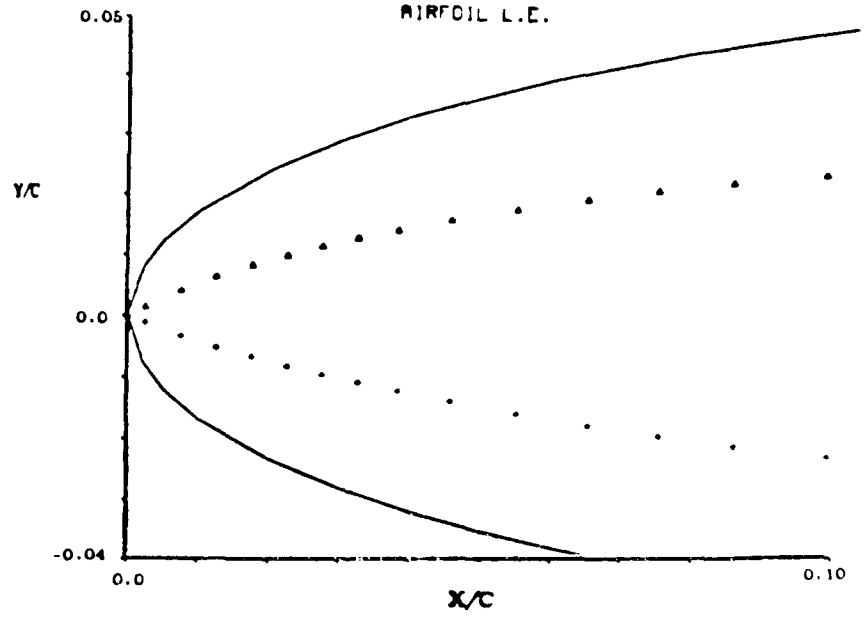

Figure 11 Geometry Comparison, NACA 0012

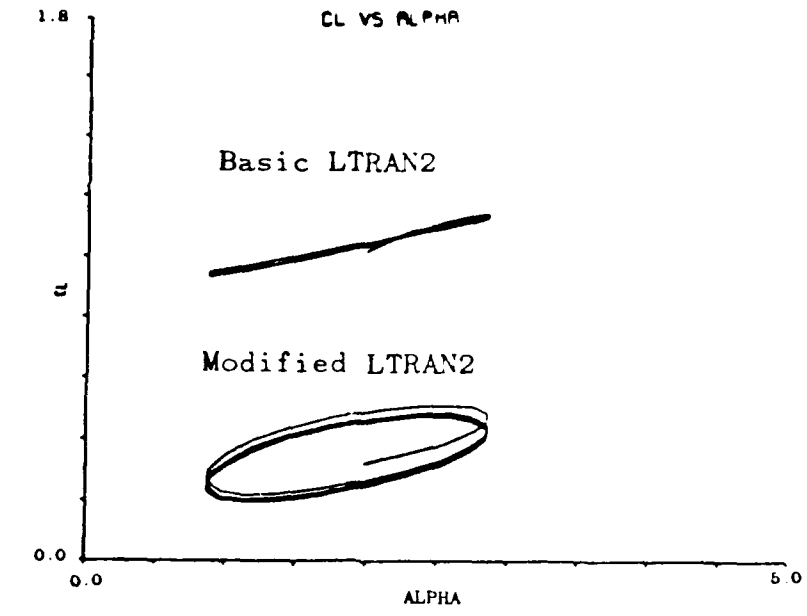

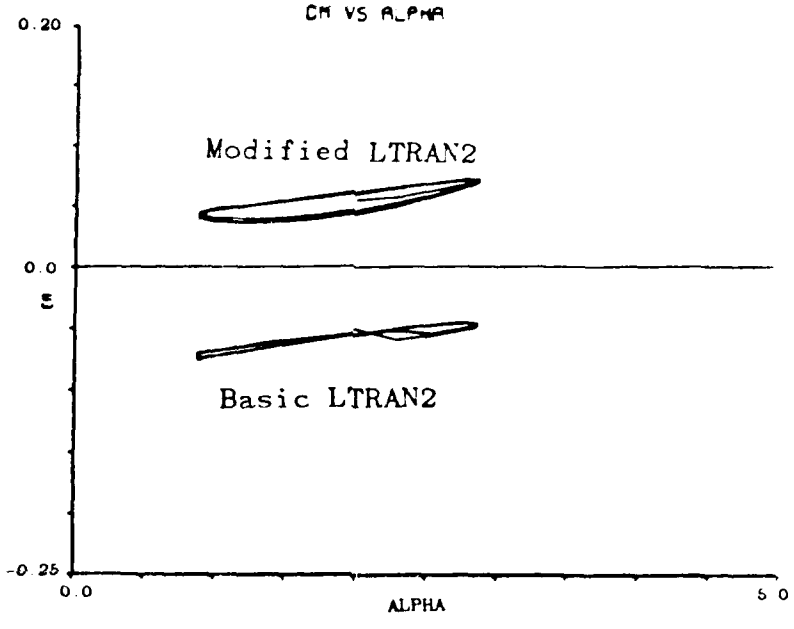

Figure 12 Lift and Pitching Moment Comparison, NACA 0012, M=0.80, k=0.20, α = 1.86 + SIN ωt

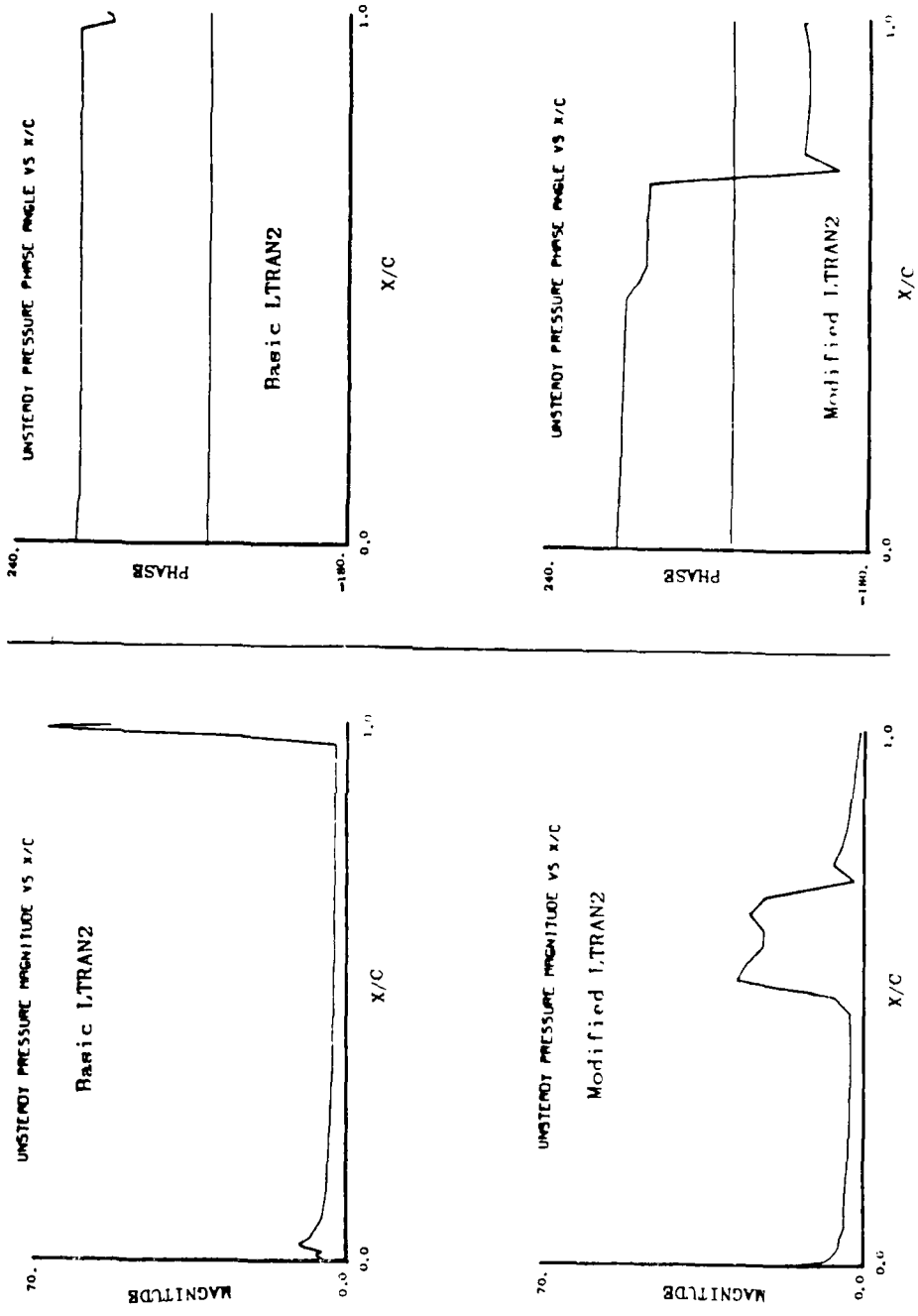

Figure 13 Comparison of Basic and Modified Geometry Results, NACA 0012, M=0.80, k=0.20, α = 1.86 + SIN ωt

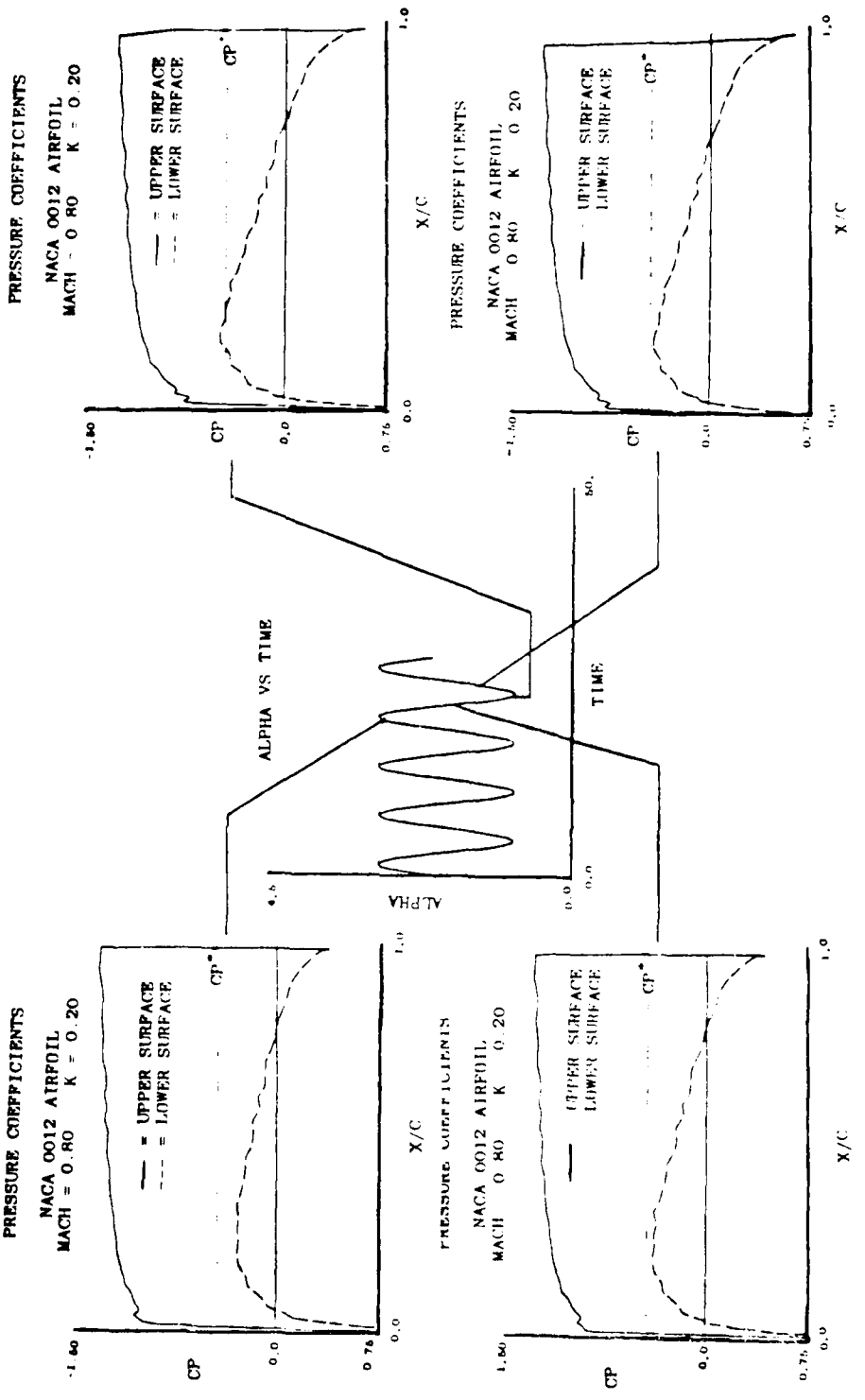

Figure 14 Basic NACA 0012 Geometry Time-Dependent Results, M=0.80, k=0.20, $\alpha = 1.86 + \text{SIN } \omega t$

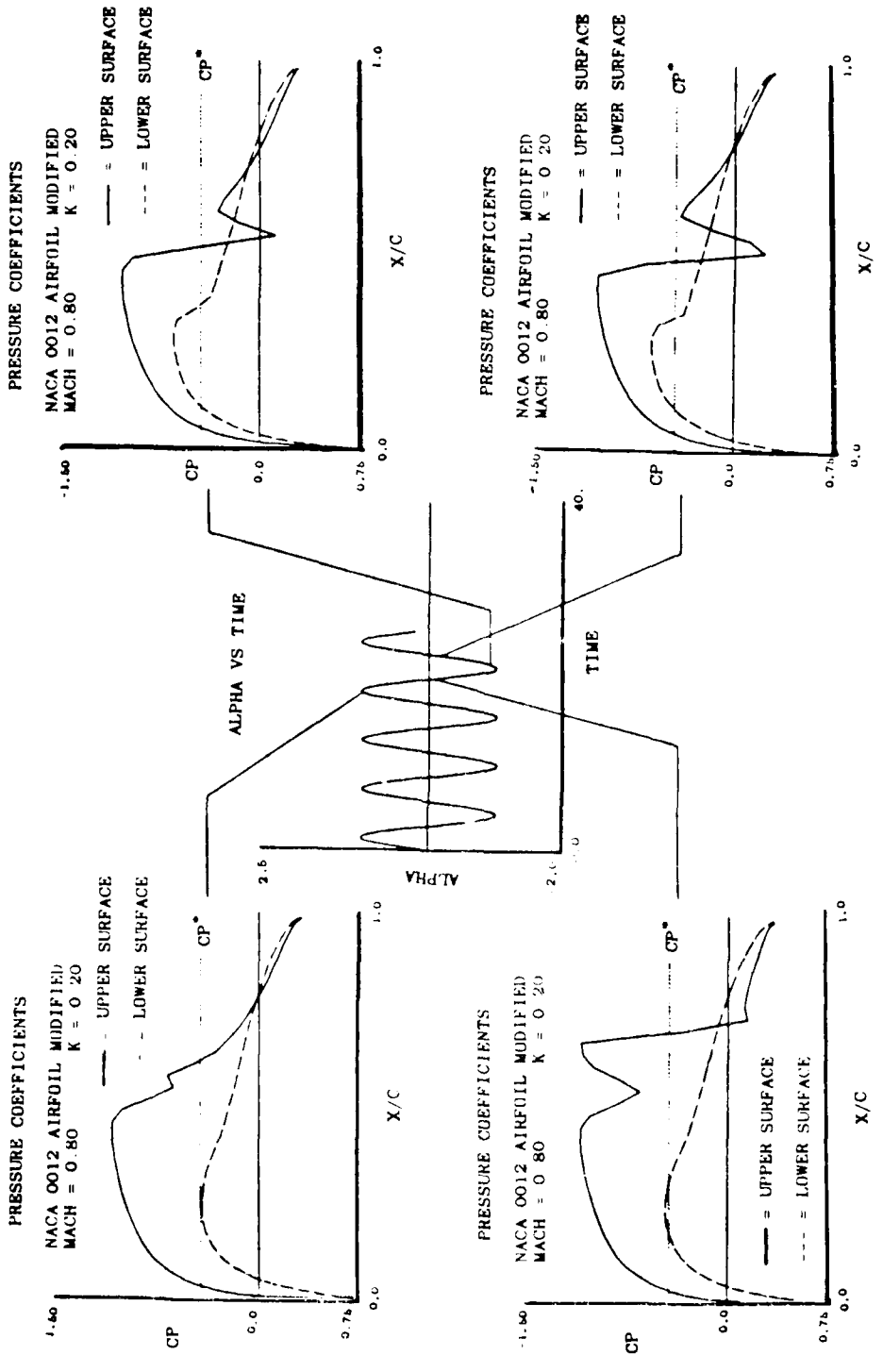

Figure 15 Modified NACA 0012 Geometry Time-Dependent Results, M=0.80, k=0.20, α = 1.86 + SIN ωt

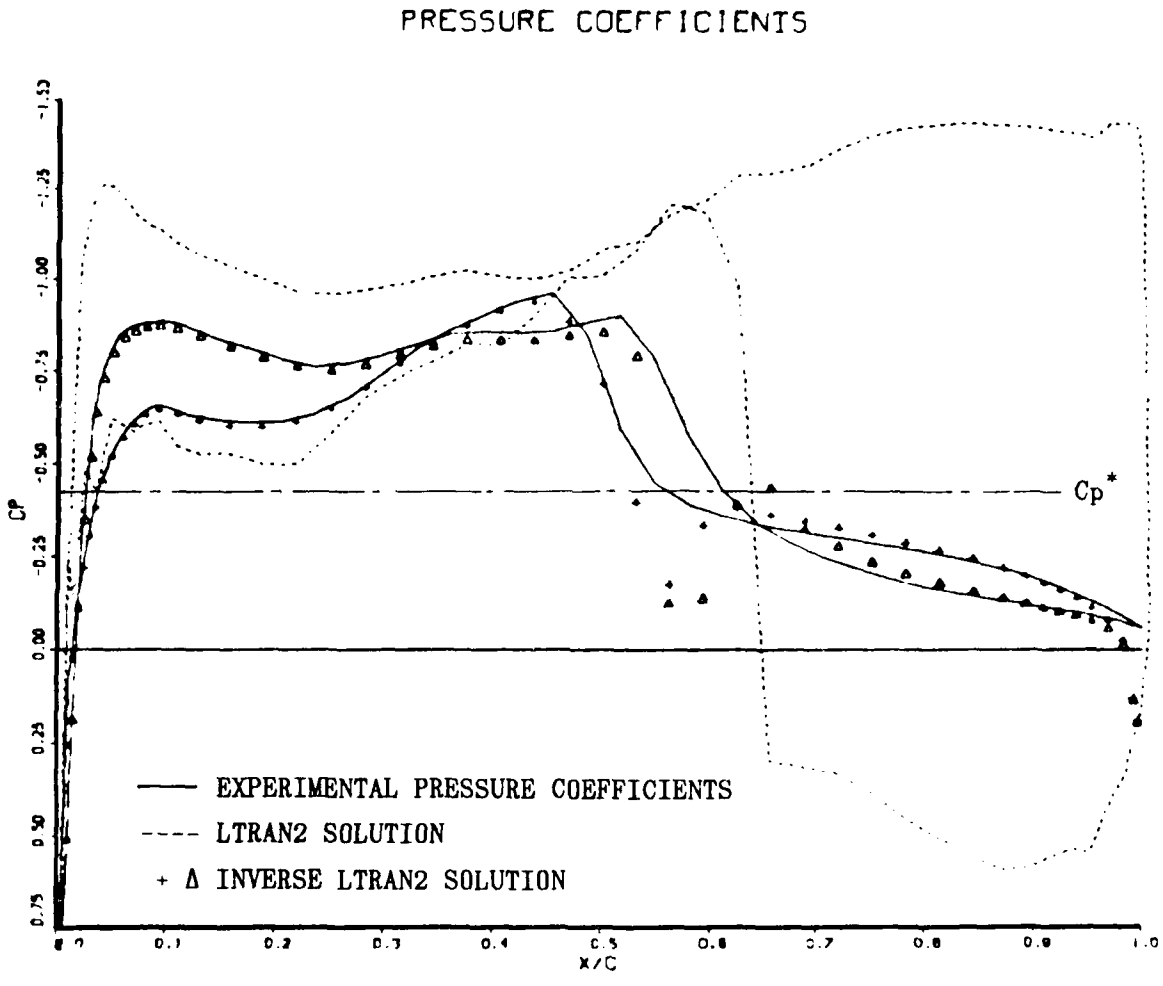

Figure 16 Pressure coefficient Comparison, NLR 7301, M=0.807, α = 0.36, $R_n = 1.2 \times 10^7$

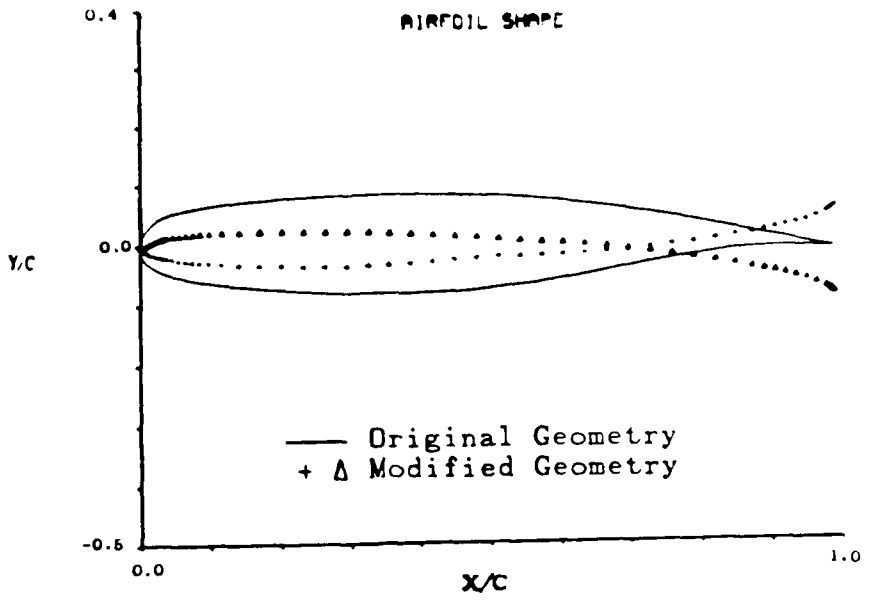

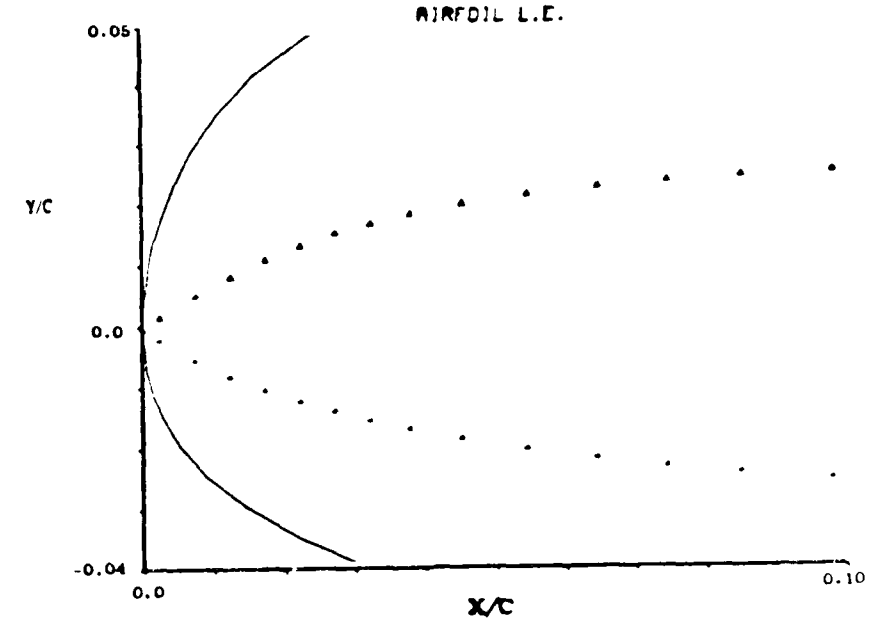

Figure 17 Geometry Comparison, NLR 7301

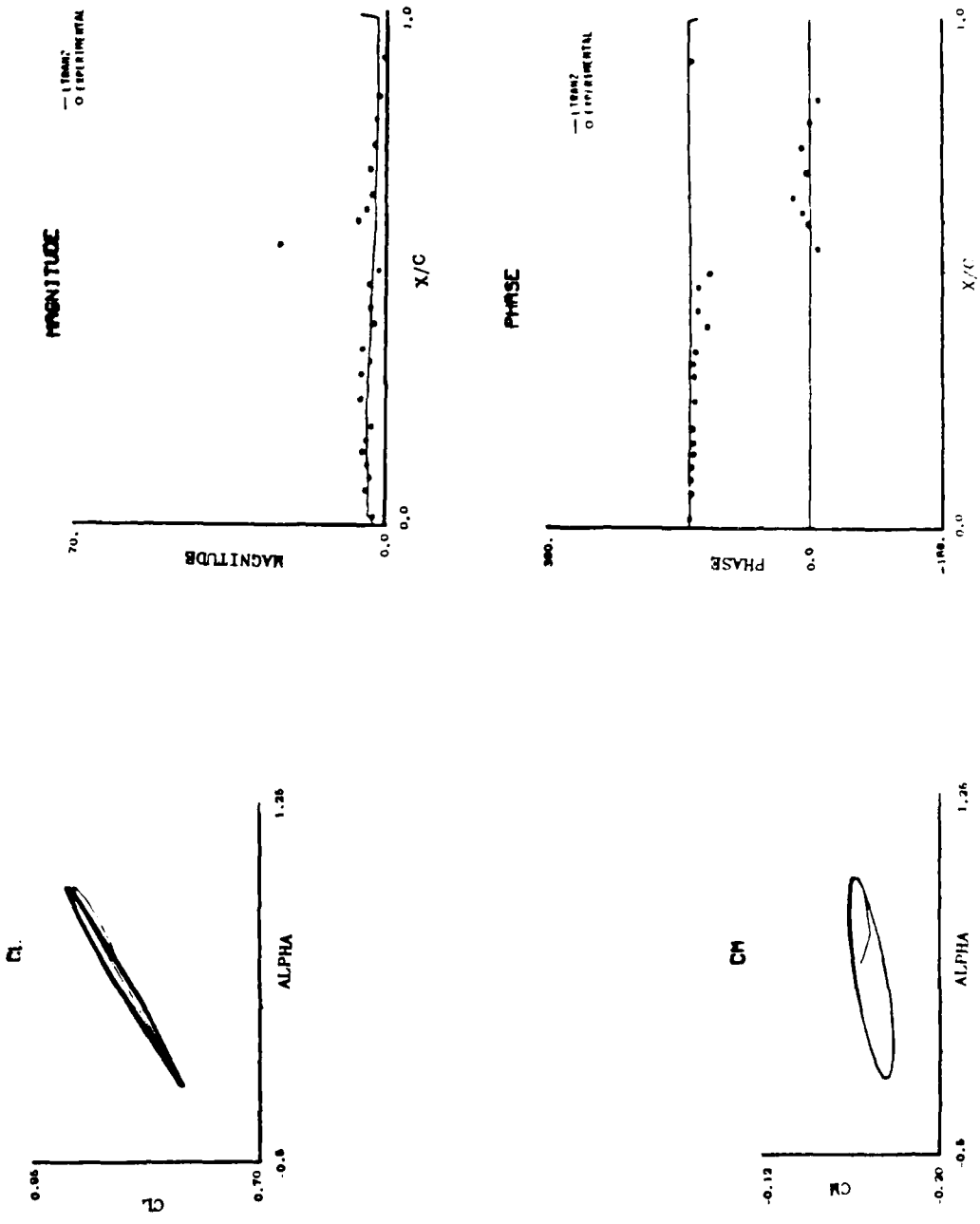

Figure 18 Comparison of Basic Geometry Results with Experimental Data, NLR 7301, M=0.807, k=0.20, α = 0.36 + 0.49 SIN ωt

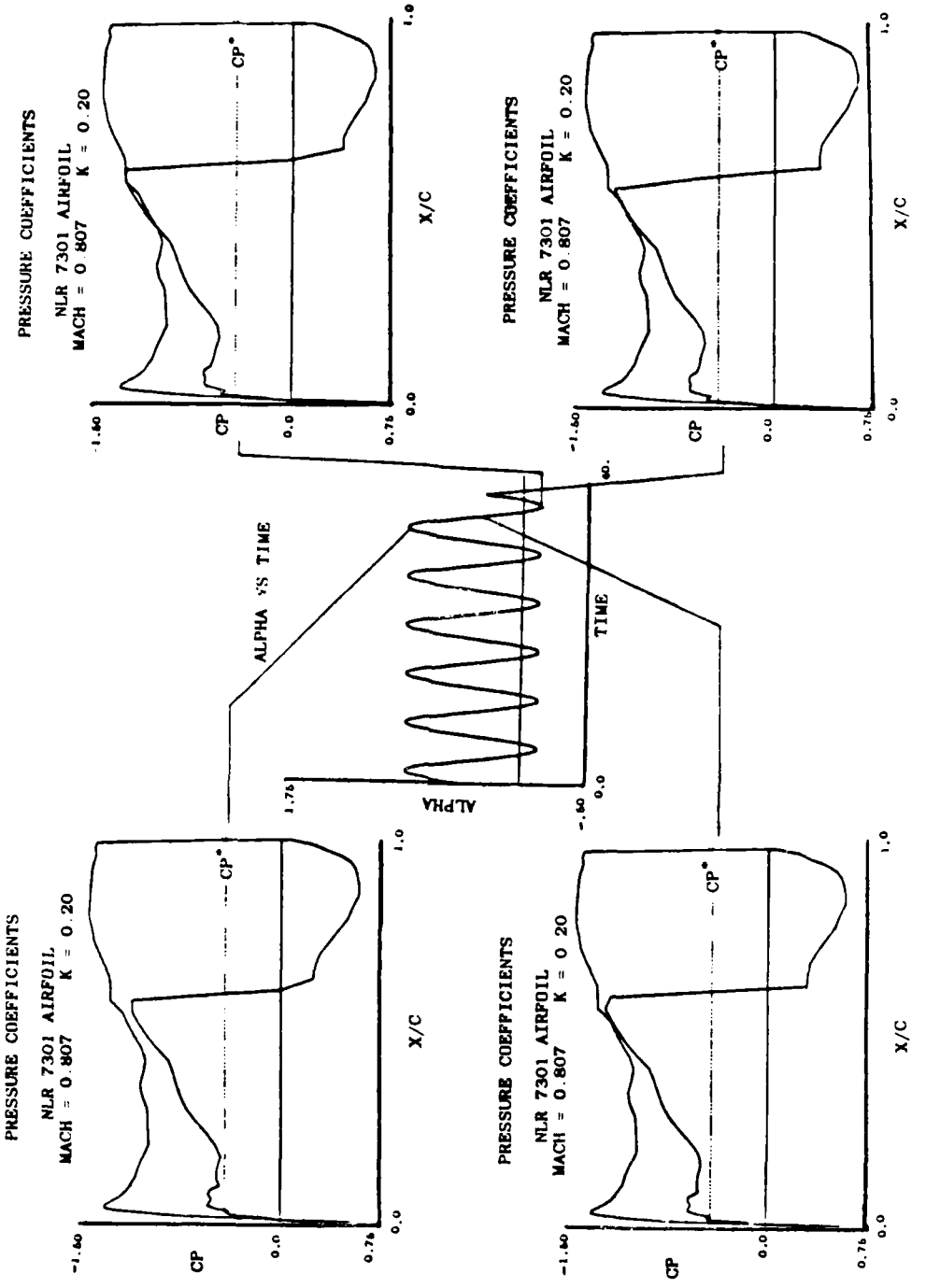

Figure 19 Basic NLR 7301 Geometry Time-Dependent Results, M=0.80, k=0.20, α = 0.36 + 0.49 SIN ωt

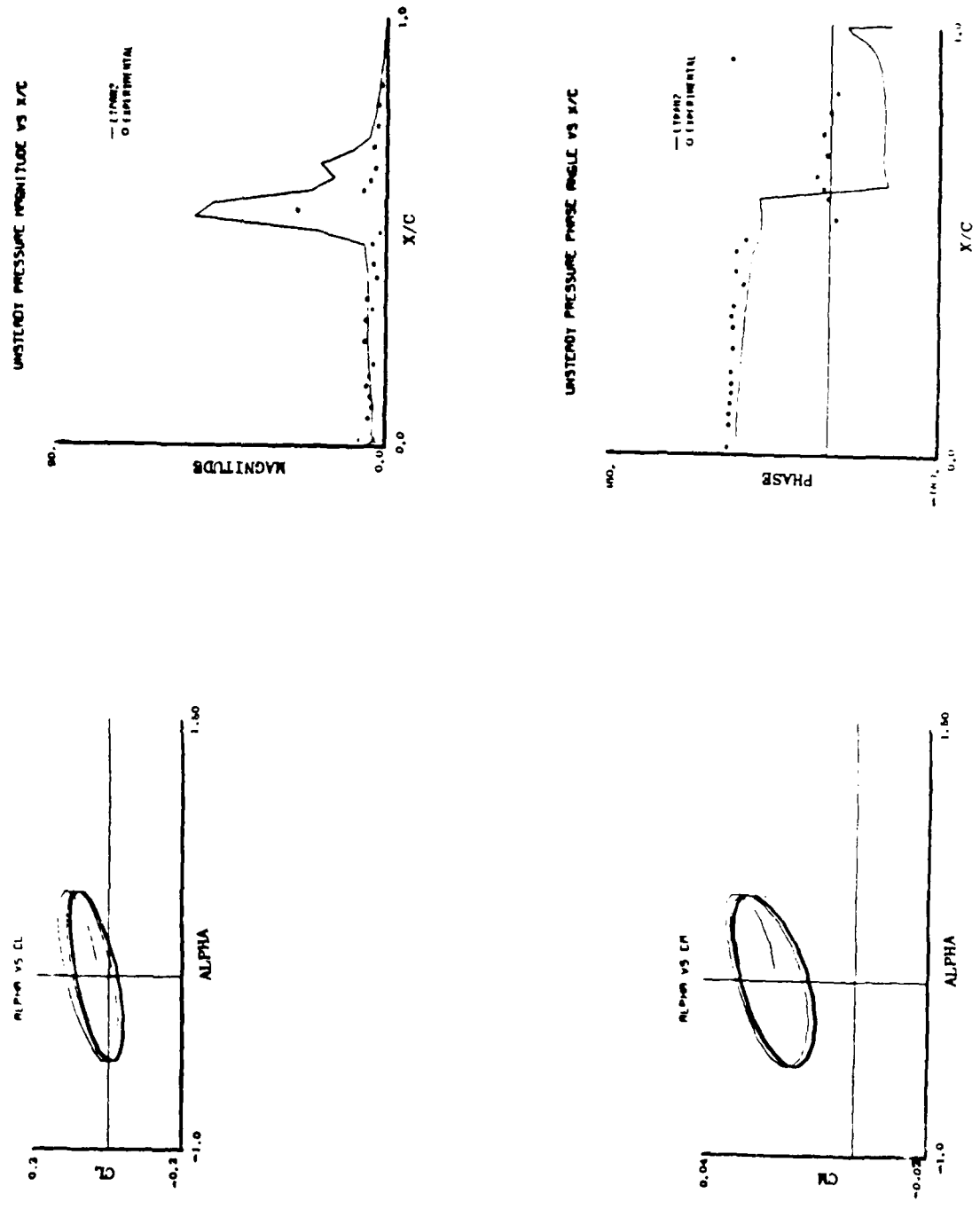

Figure 20 Comparison of Modified Geometry Results with Experimental Data, M=0.807, k=0.20, α = 0.36 + 0.49 SIN ωt

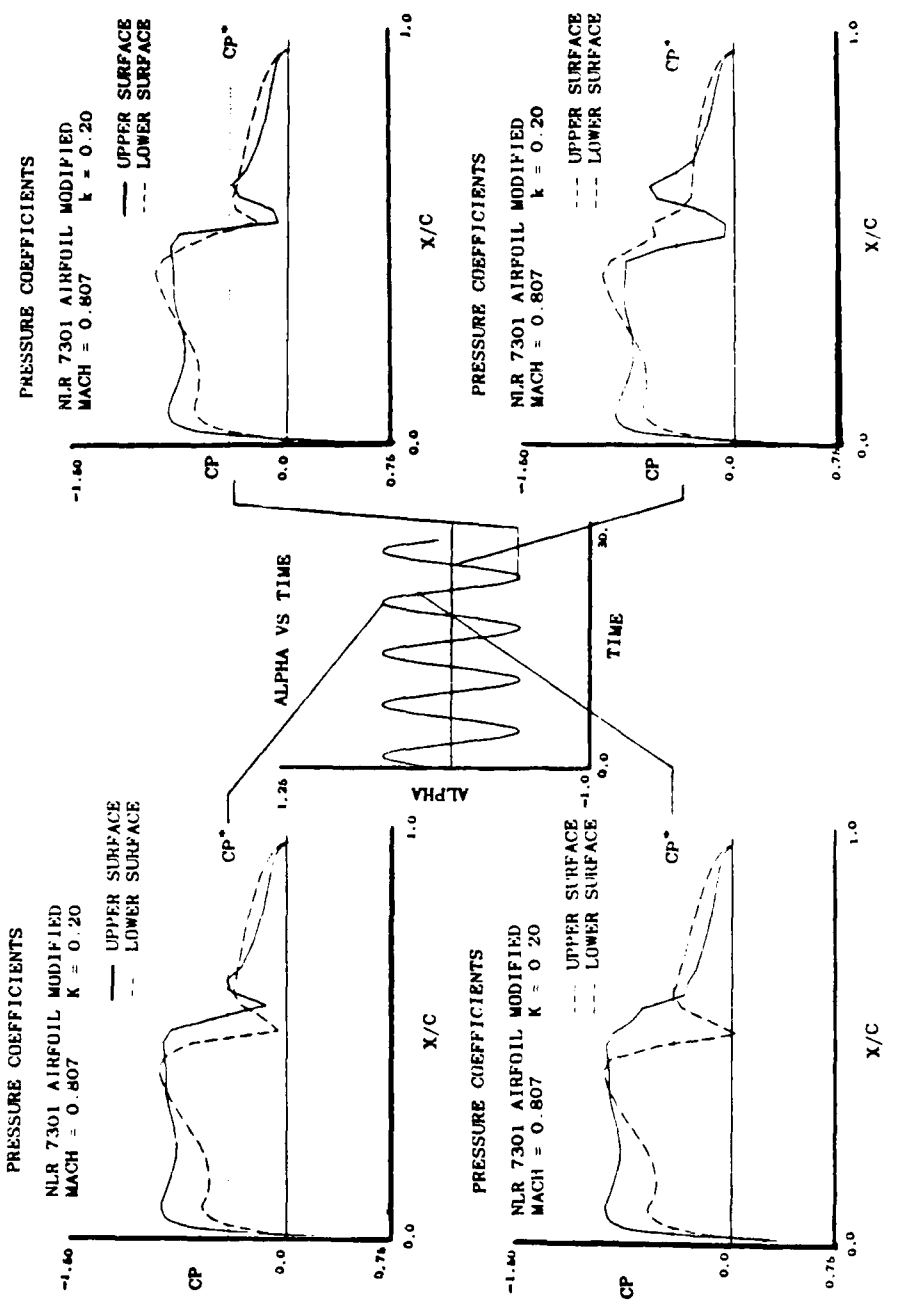

Figure 21 Modified NLR 7301 Geometry Time-Dependent Results, M=0.807, k=0.20, α = 0.36 + 0.49 Sin ωt

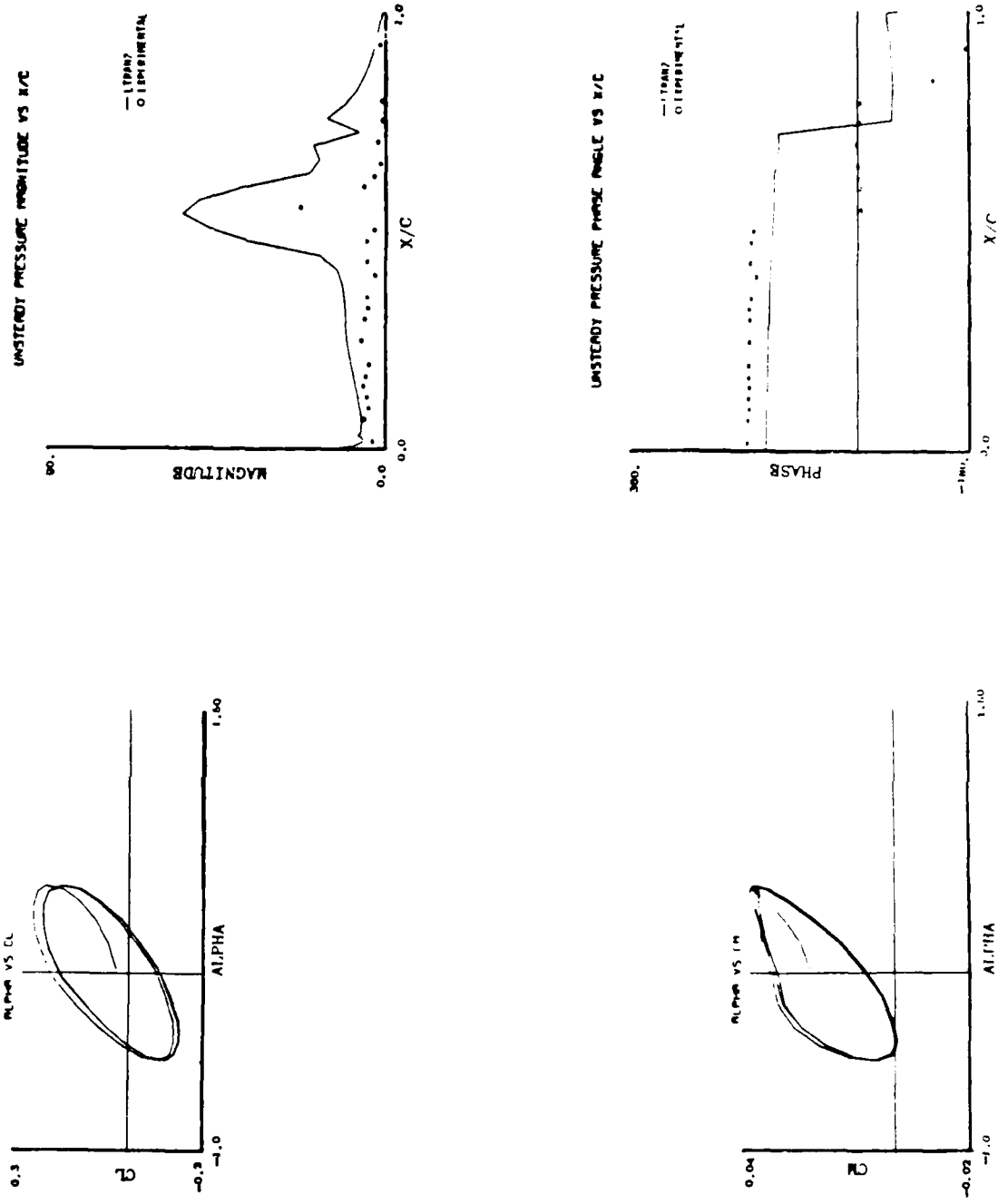

Figure 22 Comparison of Modified Geometry Results with Experimental Data, M=0.807, k=0.05, α =0.36 + SIN ωt

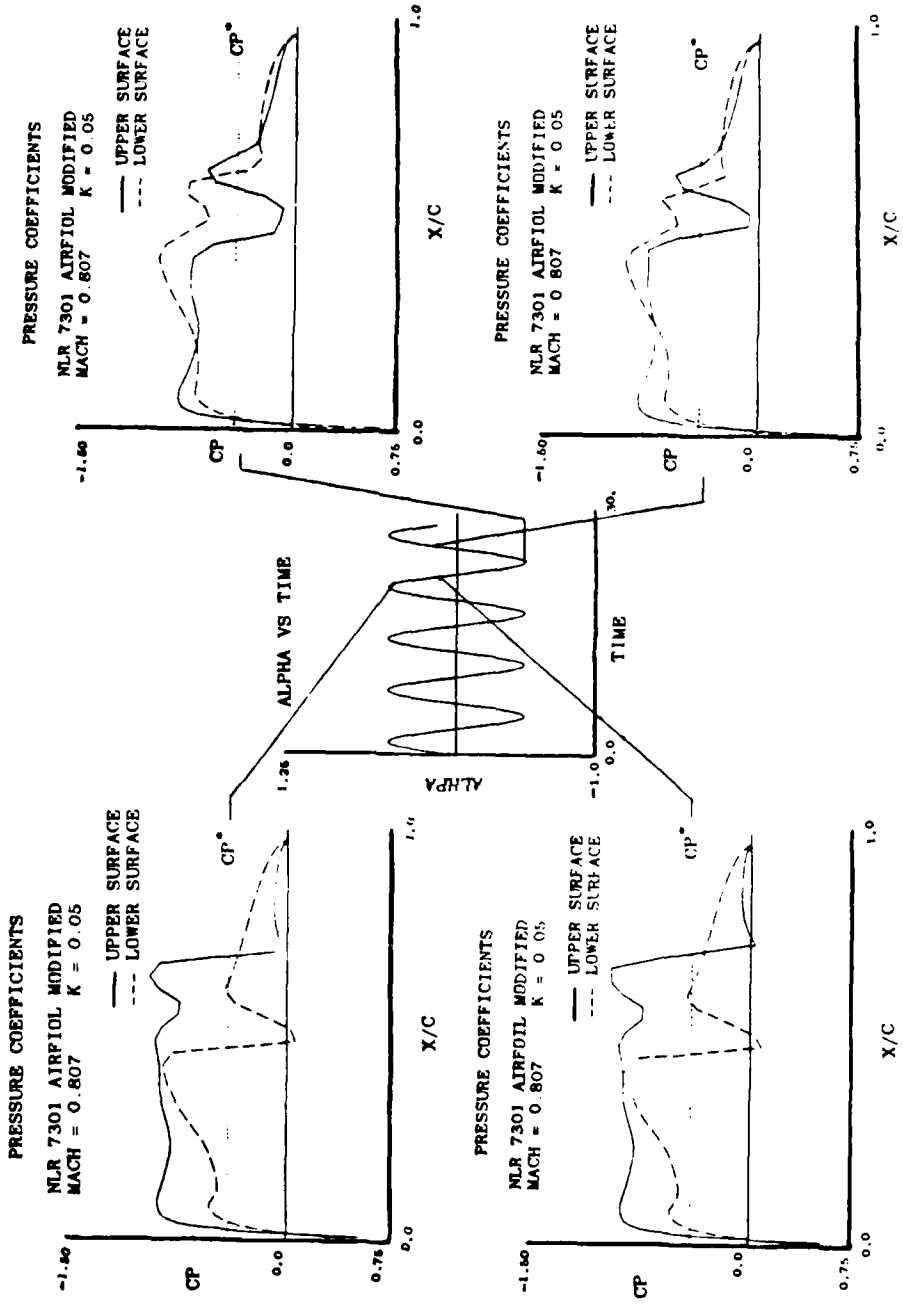

Figure 23 Modified NLR 7301 Geometry Time-Dependent Results, M=0.807, k=0.05, α = 0.36 + 0.49 SIN ωt

LIST OF SYMBOLS

A	Small disturbance equation constant $=k^2 M_\infty^2 / \tau^{2/3}$
a	Speed of sound.
AF2	Approximate factorization scheme 2.
AOA	Angle of attack.
B	Small disturbance equation constant $=k M_\infty^2 / \tau^{2/3}$
b	Boundary condition vector in AF2.
C	TSD equation $=[(1-M_\infty^2)/\tau^{2/3}]-(\gamma+1)M_\infty^m \phi_x$
c	Airfoil chord length.
C_L or CL	Lift coefficient.
C_m or CM	Pitching moment coefficient about 0.25c.
C_p or CP	Pressure coefficient.
C_p^*	Pressure coefficient corresponding to sonic flow.
C_{p_R}	Real part of complex pressure coefficient.
C_{p_I}	Imaginary part of complex pressure coefficient.
C_{p_M}	Magnitude of complex pressure coefficient = $(C_{p_R}^2 + C_{p_I}^2)^{1/2}$
f	Function that defines the airfoil geometry.
F	Intermediate result for the two step iteration process.
k	Reduced frequency $=\omega\ c/U_\infty$
L	Linear operator.
LTRAN2	Unsteady small disturbance solution procedure.
M	Mach number.
m	Exponent for Mach number (real number between 1 and 2).
N	Operator used in the AF2 development.
NSUP	Number of supersonic points.

LIST OF SYMBOLS

O	Of the order of what follows in brackets
Q	Number of parameters in the acceleration sequence.
R	Residual in the AF2 procedure.
R_n	Reynolds number (per foot).
t	Time variable.
U	Freestream velocity.
x	Cartesian coordinate in the streamwise direction.
x_0	Chord location about which the forced oscillations occur.
X/C	Chord location in fraction of chord.
y	Cartesian coordinate perpendicular to the freestream.
Y/C	Vertical coordinate in fraction of chord.

Greek

α	Angle of attack.
β	Acceleration parameter used in AF2 solution algorithm.
α_0	Angle of attack about which the oscillations occur.
α_1	Multiplier for the trig function describing the oscillations.
α_h	Upper bound for the acceleration parameters.
α_l	Lower bound for the acceleration parameters.
τ	Thickness to chord ratio for the airfoil.
δ	Partial derivative operator (with a spatial or temporal subscript).
ω	Oscillatory frequency.
Φ	Velocity potential.
ϕ	Small perturbation velocity potential.

LIST OF SYMBOLS

γ	Ratio of specific heats.
σ	Relaxation parameter for the AF2 solution algorithm.
θ	Phase angle for complex pressure coefficient = $\mathrm{Tan}^{-1}(C_{P_R}/C_{P_I})$

Subscripts

∞	Infinity or far field conditions.
x	Derivative with respect to the x coordinate.
y	Derivative with respect to the y coordinate.
t	Derivative with respect to time.
i	Index of the computational grid in the y direction.
I	i index at the airfoil.
j	Index of the computational grid in the x direction.
J	j index at the airfoil leading edge.
k	Index for the acceleration parameters.

Superscripts

n	Iteration counter for the AF2 solution procedure.
$\rightarrow$	Forward difference.
$\leftarrow$	Backward difference.
'	Derivative with respect to the x coordinate.

☆ U.S. GOVERNMENT PRINTING OFFICE 1988 - 548-054-80835